A numerical model for multiphase liquid–vapor–gas flows with interfaces and cavitation

Marica Pelanti, Keh-Ming Shyue

Version of Record: https://www.sciencedirect.com/science/article/pii/S0301932218306402
Manuscript_399fb175368cc92898ca3af23bde5ac9

A numerical model for multiphase liquid-vapor-gas flows with interfaces and cavitation

Marica Pelanti*,[a], Keh-Ming Shyue[b]

[a] *Institute of Mechanical Sciences and Industrial Applications, UMR 9219 ENSTA ParisTech - EDF - CNRS - CEA, 828, Boulevard des Maréchaux, 91762 Palaiseau Cedex, France*
[b] *Institute of Applied Mathematical Sciences and Department of Mathematics, National Taiwan University, Taipei 10617, Taiwan*

Abstract

We are interested in multiphase flows involving the liquid and vapor phases of one species and a third inert gaseous phase. We describe these flows by a hyperbolic single-velocity multiphase flow model composed of the phasic mass and total energy equations, the volume fraction equations, and the mixture momentum equation. The model includes stiff mechanical and thermal relaxation source terms for all the phases, and chemical relaxation terms to describe mass transfer between the liquid and vapor phases of the species that may undergo transition. First, we present an analysis of the characteristic wave speeds associated to the hierarchy of relaxed multiphase models corresponding to different levels of activation of infinitely fast relaxation processes, showing that sub-characteristic conditions hold. We then propose a mixture-energy-consistent finite volume method for the numerical solution of the multiphase model system. The homogeneous portion of the equations is solved numerically via a second-order wave propagation scheme based on robust HLLC-type Riemann solvers. Stiff relaxation source terms are treated by efficient numerical procedures that exploit algebraic equilibrium conditions for the relaxed states. We present numerical results for several three-phase flow problems, including two-dimensional simulations of liquid-vapor-gas flows with interfaces and cavitation phenomena.

Key words: Multiphase compressible flows, relaxation processes, liquid-vapor phase transition, finite volume schemes, Riemann solvers.
2000 MSC: 65M08, 76T10

1. Introduction

Liquid-vapor flows are found in a large variety of industrial and technological processes and natural phenomena. Often these flows involve one or more additional inert gas phases. For instance, in some processes the dynamics of a liquid-vapor mixture is coupled to the dynamics of defined regions of a third non-condensable gaseous component. An example is given by underwater explosion phenomena, where a high pressure bubble of combustion gases triggers

*Corresponding author. Tel.: +33 1 69 31 98 19; Fax: +33 1 69 31 99 97.
Email addresses: marica.pelanti@ensta-paristech.fr (Marica Pelanti), shyue@math.ntu.edu.tw (Keh-Ming Shyue)

cavitation phenomena in water [11, 24]. In other cases liquid-vapor mixtures may contain a diluted inert gas component, which may affect the flow features, such as in fuel injectors [6]. We are interested here in the simulation of this type of multiphase flows involving the liquid and vapor phases of one species and one or more additional non-condensable gaseous phases. We describe these multiphase flows by a hyperbolic single-velocity compressible flow model with infinite-rate mechanical relaxation, which extends the two-phase model that we have studied in previous work [45]. This model is composed of the phasic mass and total energy equations, the volume fraction equations, and the mixture momentum equation. The model includes thermal relaxation terms to account for heat transfer processes between all the phases, and chemical relaxation terms to describe mass transfer between the liquid and vapor phases of the species that may undergo transition. Similar hyperbolic multiphase flow models with instantaneous pressure relaxation have been previously presented for instance in [48, 27, 64]. A first contribution of our work is a rigorous derivation of the reduced pressure-relaxed model resulting from the parent non-equilibrium multiphase flow model with heat and mass transfer terms in the limit of instantaneous mechanical relaxation. This is done by following the asymptotic analysis technique employed by Murrone and Guillard [41] for the two-phase case with no heat and mass transfer. Moreover, we present an original analysis of the characteristic wave speeds associated to the hierarchy of relaxed multiphase models corresponding to different levels of activation of infinitely fast mechanical and thermo-chemical relaxation processes. Similar to results shown in the literature for the two-phase case [18, 36, 32], we demonstrate that sub-characteristic conditions hold, namely the speed of sound of the multiphase mixture is reduced whenever an additional equilibrium assumption is introduced. Then, we present a finite volume method for the numerical solution of the multiphase model system based on a classical fractional step procedure. The homogeneous hyperbolic portion of the equations is solved numerically via a second-order accurate wave propagation scheme, which employs a HLLC-type Riemann solver. In particular, we present here a new generalized HLLC-solver based on the idea of the Suliciu relaxation solver of [8], extending the solver that we have recently proposed in [15] for the two-phase case. This HLLC/Suliciu-type solver allows us to guarantee positivity preservation with a suitable choice of the wave speeds. Stiff relaxation source terms are treated by efficient numerical procedures that exploit algebraic equilibrium conditions for the relaxed states, following the ideas of our work [45]. Similar approaches have been previously presented in the literature for instance in [27]. One important property of our numerical method is *mixture-energy-consistency* in the sense defined in [45], that is the method guarantees conservation of the mixture total energy at the discrete level, and it guarantees consistency by construction of the values of the relaxed states with the mixture pressure law. This property is ensured thanks to the total-energy-based formulation of the model system. We present several numerical results for three-phase flow problems, including problems involving liquid-vapor-gas flows with interfaces and cavitation phenomena, such as underwater explosion tests.

This article is organized as follows. In Section 2 we present the multiphase flow model under study. In Section 3 we derive the limit pressure-equilibrium model associated to the considered multiphase flow model, and we analyze the characteristic speeds of the relaxed models in the hierarchy stemming from the parent relaxation model. In Section 4 we illustrate the numerical method that we have developed to solve the multiphase flow equations. Several one-dimensional and two-dimensional numerical experiments are finally presented in Section 5.

2. Single-velocity multiphase compressible flow model

We consider an inviscid compressible flow composed of N phases that we assume in kinematic equilibrium with velocity $\vec{u}$. In this work we are mainly interested in three-phase flows, $N = 3$, nonetheless we shall present here a general multiphase flow formulation. The volume fraction, density, internal energy per unit volume, and pressure of each phase will be denoted by α_k , ρ_k , $\mathcal{E}_k$, p_k , $k = 1, \dots, N$, respectively. We will denote the total energy for the kth phase with $E_k = \mathcal{E}_k + \rho_k \frac{|\vec{u}|^2}{2}$. The saturation condition is $\sum_{k=1}^{N} \alpha_k = 1$. The mixture density is $\rho = \sum_{k=1}^{N} \alpha_k \rho_k$, the mixture internal energy is $\mathcal{E} = \sum_{k=1}^{N} \alpha_k \mathcal{E}_k$, and the mixture total energy is $E = \sum_{k=1}^{N} \alpha_k E_k = \mathcal{E} + \rho \frac{|\vec{u}|^2}{2}$. Moreover, we will denote the kth specific internal energy with $\varepsilon_k = \mathcal{E}_k / \rho_k$. Mechanical and thermal transfer processes are considered in general for all the phases. We assume that one species in the mixture can undergo phase transition, so that it can exist as a vapor or a liquid phase, and mass transfer terms are accounted for this species only. We will use the subscripts 1 and 2 to denote the liquid and vapor phases of this species. We describe the N-phase flow under consideration by a compressible flow model that extends the six-equation two-phase flow system that we studied in [45]. The model system is composed of the volume fraction equations for $N - 1$ phases, the mass and total energy equations for all the N phases, and d mixture momentum equations, where d denotes the spatial dimension:

$$\partial_t \alpha_k + \vec{u} \cdot \nabla \alpha_k = \textstyle\sum_{j=1}^{N} \mathcal{P}_{kj} , \quad k = 1, 3, \dots, N, \tag{1a}$$

$$\partial_t (\alpha_1 \rho_1) + \nabla \cdot (\alpha_1 \rho_1 \vec{u}) = \mathcal{M} , \tag{1b}$$

$$\partial_t (\alpha_2 \rho_2) + \nabla \cdot (\alpha_2 \rho_2 \vec{u}) = -\mathcal{M} , \tag{1c}$$

$$\partial_t (\alpha_k \rho_k) + \nabla \cdot (\alpha_k \rho_k \vec{u}) = 0 , \quad k = 3, \dots, N , \tag{1d}$$

$$\partial_t (\rho \vec{u}) + \nabla \cdot \left[\rho \vec{u} \otimes \vec{u} + \left(\textstyle\sum_{k=1}^{N} \alpha_k p_k \right) \mathbb{I} \right] = 0 , \tag{1e}$$

$$\partial_t (\alpha_1 E_1) + \nabla \cdot (\alpha_1 (E_1 + p_1) \vec{u}) + \Upsilon_1 = - \textstyle\sum_{j=1}^{N} p_{\mathrm{I}1j} \mathcal{P}_{1j} + \sum_{j=1}^{N} Q_{1j} + \left(g_{\mathrm{I}} + \frac{|\vec{u}|^2}{2} \right) \mathcal{M} , \tag{1f}$$

$$\partial_t (\alpha_2 E_2) + \nabla \cdot (\alpha_2 (E_2 + p_2) \vec{u}) + \Upsilon_2 = - \textstyle\sum_{j=1}^{N} p_{\mathrm{I}2j} \mathcal{P}_{2j} + \sum_{j=1}^{N} Q_{2j} - \left(g_{\mathrm{I}} + \frac{|\vec{u}|^2}{2} \right) \mathcal{M} , \tag{1g}$$

$$\partial_t (\alpha_k E_k) + \nabla \cdot (\alpha_k (E_k + p_k) \vec{u}) + \Upsilon_k = - \textstyle\sum_{j=1}^{N} p_{\mathrm{I}kj} \mathcal{P}_{kj} + \sum_{j=1}^{N} Q_{kj} , \quad k = 3, \dots, N . \tag{1h}$$

The non-conservative terms Υ_k appearing in the phasic total energy equations (1f)–(1h) are given by

$$\Upsilon_k = \vec{u} \cdot \left[Y_k \nabla \left(\textstyle\sum_{j=1}^{N} \alpha_j p_j \right) - \nabla (\alpha_k p_k) \right] , \quad k = 1, \dots, N , \tag{1i}$$

where $Y_k = \frac{\alpha_k \rho_k}{\rho}$ denotes the mass fraction of phase k. In the system above $\mathcal{P}_{kj}$ and Q_{kj} represent the volume transfer and the heat transfer, respectively, between the phases k and j, $k, j = 1, \dots, N$. The term $\mathcal{M}$ indicates the mass transfer between the liquid and vapor phases indexed with 1 and 2. The transfer terms are defined as relaxation terms:

$$\mathcal{P}_{kj} = \mu_{kj} (p_k - p_j) , \quad Q_{kj} = \vartheta_{kj} (T_j - T_k) , \quad \mathcal{M} = \nu (g_2 - g_1) , \tag{2}$$

where T_k denotes the phasic temperature, g_k the phasic chemical potential, and where we have introduced the mechanical, thermal and chemical relaxation parameters $\mu_{kj} = \mu_{jk} \geq 0$, $\vartheta_{kj} = \vartheta_{jk} \geq 0$, and $\nu = \nu_{12} = \nu_{21} \geq 0$, respectively. Note that $\mathcal{P}_{kj} = -\mathcal{P}_{jk}$ and $Q_{kj} = -Q_{jk}$. The quantities $p_{\mathrm{I}kj} = p_{\mathrm{I}jk}$ are interface pressures and g_{I} is an interface chemical potential. We shall assume that all mechanical relaxation processes are infinitely fast, $\mu_{kj} = \mu_{jk} \equiv \mu \to +\infty$, so

that mechanical equilibrium is attained instantaneously between all the phases. Indeed here, following the same idea of [51, 52, 45], the parent non-equilibrium multiphase flow model with instantaneous pressure relaxation is used to approximate solutions to the limiting pressure-equilibrium flow model, which is the physical flow model of interest. Concerning thermal and chemical relaxation, following the simple approach of [51], we consider in this work that these processes are either inactive, $\vartheta_{kj} = 0$, $\nu = 0$, or they act infinitely fast, $\vartheta_{kj} \to +\infty$, $\nu \to +\infty$. Heat and mass transfer may be activated at selected locations, for instance at interfaces for a phase pair (k, j), identified by $\min(\alpha_k, \alpha_j) > \epsilon$, where ϵ is a tolerance.

The closure of the system (1) is obtained through the specification of an equation of state (EOS) for each phase $p_k = p_k(\mathcal{E}_k, \rho_k)$, $T_k = T_k(p_k, \rho_k)$. For the numerical model here we will adopt the widely used stiffened gas (SG) equation of state [39]:

$$p_k(\mathcal{E}_k, \rho_k) = (\gamma_k - 1)\mathcal{E}_k - \gamma_k \varpi_k - (\gamma_k - 1)\eta_k \rho_k \,, \tag{3a}$$

$$T_k(p_k, \rho_k) = \frac{p_k + \varpi_k}{\kappa_{vk}\rho_k(\gamma_k - 1)}, \tag{3b}$$

where γ_k, ϖ_k, η_k and κ_{vk} are constant material-dependent parameters. In particular, κ_{vk} represents the specific heat at constant volume. The corresponding expression for the phasic entropy is

$$s_k = \kappa_{vk} \log(T_k^{\gamma_k}(p_k + \varpi_k)^{-(\gamma_k - 1)}) + \eta_k' \,, \tag{3c}$$

where η_k' = constant, and $g_k = h_k - T_k s_k$, with h_k denoting the phasic specific enthalpy. The parameters for the SG EOS for the liquid and vapor phases of the species that may undergo transition are determined so that the theoretical saturation curve defined by $g_1 = g_2$ matches the experimental one for the considered material [26]. The mixture pressure law for the model with instantaneous pressure relaxation is determined by the mixture energy relation

$$\mathcal{E} = \sum_{k=1}^{N} \alpha_k \mathcal{E}_k(p, \rho_k), \tag{4}$$

where we have used the mechanical equilibrium conditions $p_k = p$, for all $k = 1, \ldots, N$, in the phasic energy laws $\mathcal{E}_k(p_k, \rho_k)$. Note that for the particular case of the SG EOS, an explicit expression of the mixture pressure can be obtained from (4).

Since here we will consider relaxation parameters either $= 0$ or $\to +\infty$, a specification of the expression for the interface quantities p_{Ikj}, g_I is not needed. Nevertheless, let us remark that the definition of these interface quantities must be consistent with the second law of thermodynamics, which requires a non-negative entropy production for the mixture. The equation for the mixture total entropy $\mathcal{S} = \rho s$, $s = \sum_{k=1}^{N} Y_k s_k$, is found as:

$$\partial_t \mathcal{S} + \nabla \cdot (\mathcal{S}\vec{u}) = \mathcal{H}_\mathcal{P} + \mathcal{H}_\mathcal{Q} + \mathcal{H}_\mathcal{M} \,, \tag{5a}$$

where

$$\mathcal{H}_\mathcal{P} = \sum_{k=1}^{N}\sum_{j=1}^{N} \frac{p_k - p_{Ikj}}{T_k}\mathcal{P}_{kj} \,, \quad \mathcal{H}_\mathcal{Q} = \sum_{k=1}^{N}\sum_{j=1}^{N} \frac{1}{T_k}\mathcal{Q}_{kj} \,, \quad \mathcal{H}_\mathcal{M} = \left(\frac{g_I - g_1}{T_1} - \frac{g_1 - g_2}{T_2}\right)\mathcal{M}. \tag{5b}$$

For consistency of the multiphase model (1) with the second law of thermodynamics we need $\mathcal{H}_\mathcal{P} + \mathcal{H}_\mathcal{Q} + \mathcal{H}_\mathcal{M} \geq 0$. By following the arguments in [18], one can infer the following sufficient consistency conditions on the interface quantities:

$$p_{Ikj} \in [\min(p_k, p_j), \max(p_k, p_j)] \quad \text{and} \quad g_I \in [\min(g_1, g_2), \max(g_1, g_2)]. \tag{6}$$

The model (1) is hyperbolic and the associated speed of sound c_f (non-equilibrium or frozen sound speed) is defined by

$$c_\mathrm{f}^2 = \left(\frac{\partial p_\mathrm{m}}{\partial \rho}\right)_{s_k, Y_k, \alpha_k, k=1,\dots,N}, \tag{7}$$

where we have introduced the mixture pressure

$$p_\mathrm{m}(\rho, s_1, \dots, s_N, Y_1, \dots, Y_{N-1}, \alpha_1, \dots, \alpha_{N-1}) = \sum_{k=1}^{N} \alpha_k p_k\left(s_k, \rho\frac{Y_k}{\alpha_k}\right). \tag{8}$$

From this definition, by noticing that

$$\left(\frac{\partial p_k}{\partial \rho}\right)_{s_k, Y_k, \alpha_k} = \left(\frac{\partial p_k}{\partial \rho_k}\right)_{s_k, Y_k, \alpha_k}\left(\frac{\partial \rho_k}{\partial \rho}\right)_{s_k, Y_k, \alpha_k} = c_k^2\frac{Y_k}{\alpha_k}, \tag{9}$$

we obtain the expression:

$$c_\mathrm{f} = \sqrt{\sum_{k=1}^{N} Y_k c_k^2}, \tag{10}$$

where $c_k = \sqrt{\left(\frac{\partial p_k}{\partial \rho_k}\right)_{s_k}}$ is the speed of sound of the phase k, which can be expressed as $c_k = \sqrt{\Gamma_k h_k + \chi_k}$, where $\Gamma_k = (\partial p_k/\partial \mathcal{E}_k)_{\rho_k}$ (Grüneisen coefficient), and $\chi_k = (\partial p_k/\partial \rho_k)_{\mathcal{E}_k}$.

3. Hierarchy of multiphase relaxed models and speed of sound

By considering different levels of activation of instantaneous relaxation processes we can establish from the model (1) a hierarchy of hyperbolic multiphase flow models. Here in particular we derive the expression of the speed of sound for the relaxed models in this hierarchy, similar to [18, 19].

3.1. p-relaxed model

In the considered limit of instantaneous mechanical relaxation $\mu_{kj} \equiv \mu \to +\infty$, the model system (1) reduces to a hyperbolic single-velocity single-pressure model, which is a generalization of the five-equation two-phase flow model of Kapila *et al.* [23]. The reduced pressure equilibrium model, which we shall also call p-relaxed model, can be derived by means of asymptotic analysis techniques, cf. in particular [41]. We show the derivation for the one-dimensional case in Appendix A. Denoting with p the equilibrium pressure, we obtain the

following relaxed system, composed of $2N + d$ equations:

$$\partial_t \alpha_1 + \vec{u}\cdot\nabla\alpha_1 = K_1 \nabla\cdot\vec{u} + \frac{\Gamma_1}{\rho_1 c_1^2}\sum_{j=2}^{N} \mathcal{Q}_{1j} - \alpha_1 \frac{\rho c_p^2}{\rho_1 c_1^2}\sum_{\substack{j,i=1\\ i>j}}^{N} \mathcal{Q}_{ji}\left(\frac{\Gamma_j}{\rho_j c_j^2} - \frac{\Gamma_i}{\rho_i c_i^2}\right)$$
$$+\frac{\rho c_p^2}{\rho_1 c_1^2}\left((\Gamma_1(g_1 - h_1) + c_1^2)\sum_{j=2}^{N}\frac{\alpha_j}{\rho_j c_j^2} + (\Gamma_2(g_1 - h_2) + c_2^2)\frac{\alpha_1}{\rho_2 c_2^2}\right)\mathcal{M}, \tag{11a}$$

$$\partial_t \alpha_k + \vec{u}\cdot\nabla\alpha_k = K_k \nabla\cdot\vec{u} + \frac{\Gamma_k}{\rho_k c_k^2}\sum_{\substack{j=1\\ j\neq k}}^{N} \mathcal{Q}_{kj} - \alpha_k \frac{\rho c_p^2}{\rho_k c_k^2}\sum_{\substack{j,i=1\\ i>j}}^{N} \mathcal{Q}_{ji}\left(\frac{\Gamma_j}{\rho_j c_j^2} - \frac{\Gamma_i}{\rho_i c_i^2}\right)$$
$$+\rho c_p^2 \frac{\alpha_k}{\rho_k c_k^2}\left(\frac{\Gamma_2(g_1 - h_2) + c_2^2}{\rho_2 c_2^2} - \frac{\Gamma_1(g_1 - h_1) + c_1^2}{\rho_1 c_1^2}\right)\mathcal{M}, \quad k = 3, \ldots, N, \tag{11b}$$

$$\partial_t(\alpha_1\rho_1) + \nabla\cdot(\alpha_1\rho_1\vec{u}) = \mathcal{M}, \tag{11c}$$

$$\partial_t(\alpha_2\rho_2) + \nabla\cdot(\alpha_2\rho_2\vec{u}) = -\mathcal{M}, \tag{11d}$$

$$\partial_t(\alpha_k\rho_k) + \nabla\cdot(\alpha_k\rho_k\vec{u}) = 0, \quad k = 3, \ldots, N, \tag{11e}$$

$$\partial_t(\rho\vec{u}) + \nabla\cdot(\rho\vec{u}\otimes\vec{u} + p\mathbb{I}) = 0, \tag{11f}$$

$$\partial_t E + \nabla\cdot((E + p)\vec{u}) = 0, \tag{11g}$$

where

$$K_k = \rho c_p^2 \alpha_k \sum_{\substack{j=1\\ j\neq k}}^{N} \alpha_j \left(\frac{1}{\rho_k c_k^2} - \frac{1}{\rho_j c_j^2}\right) = \alpha_k\left(\frac{\rho c_p^2}{\rho_k c_k^2} - 1\right). \tag{12}$$

In the relations above we have introduced the pressure equilibrium speed of sound c_p (a generalization of Wood's sound speed), defined by

$$c_p^2 = \left(\frac{\partial p}{\partial \rho}\right)_{s_1,\ldots,s_N,Y_1,\ldots,Y_N}, \tag{13}$$

from which we obtain the expression:

$$c_p = \left(\rho\sum_{k=1}^{N}\frac{\alpha_k}{\rho_k c_k^2}\right)^{-\frac{1}{2}}. \tag{14}$$

As we mentioned above, the pressure equilibrium model (1) is indeed the physical flow model of interest. Similar to the two-phase case [52, 63, 45], the non-equilibrium model (11) with instantaneous mechanical relaxation is convenient to approximate numerically solutions to the p-relaxed model.

Remark 1. For the two-phase case $N = 2$ the p-relaxed model (11) has a form analogous to the pressure-equilibrium model presented by Saurel *et al.* in [51], nonetheless we remark a difference in the expression of mass transfer term appearing in the volume fraction equation. The equation for α_1 obtained from (11) for $N = 2$ can be written as:

$$\partial_t\alpha_1 + \vec{u}\cdot\nabla\alpha_1 = K_1\nabla\cdot\vec{u} + \zeta\left(\frac{\Gamma_1}{\alpha_1} + \frac{\Gamma_2}{\alpha_2}\right)\mathcal{Q} + \zeta\left(\frac{\Gamma_1(g_1 - h_1) + c_1^2}{\alpha_1} + \frac{\Gamma_2(g_1 - h_2) + c_2^2}{\alpha_2}\right)\mathcal{M}, \tag{15}$$

where $K_1 = \zeta(\rho_2 c_2^2 - \rho_1 c_1^2)$ and $\zeta = \frac{\alpha_1\alpha_2}{\alpha_2\rho_1 c_1^2 + \alpha_1\rho_2 c_2^2}$. The equation for the volume fraction α_1 of the relaxed pressure-equilibrium model reported in [51] is:

$$\partial_t\alpha_1 + \vec{u}\cdot\nabla\alpha_1 = K_1\nabla\cdot\vec{u} + \zeta\left(\frac{\Gamma_1}{\alpha_1} + \frac{\Gamma_2}{\alpha_2}\right)\mathcal{Q} + \zeta\left(\frac{c_1^2}{\alpha_1} + \frac{c_2^2}{\alpha_2}\right)\mathcal{M}. \tag{16}$$

We observe that the two formulations are equivalent only with the following definition of the interface chemical potential g_I:

$$g_\mathrm{I} = \frac{\alpha_2\Gamma_1 h_1 + \alpha_1\Gamma_2 h_2}{\alpha_2\Gamma_1 + \alpha_1\Gamma_2}\,. \tag{17}$$

This definition in general does not satisfy the sufficient condition for entropy consistency (6). Nevertheless, let us note that the numerical model in [51] considers either no mass transfer or infinite-rate mass transfer, so that the factor multiplying $\mathcal{M}$ in (16) has no influence in these specific circumstances.

Remark 2. In our previous work [45] an additional term of the form $\mathcal{M}/\rho_\mathrm{I}$ was written in the volume fraction equation of the six-equation two-phase flow model corresponding to (1) for $N = 2$, with ρ_I representing an interface density. Similar to [18], this term is not included in the present multiphase model (1). The purpose of the term $\mathcal{M}/\rho_\mathrm{I}$ in [45] was to indicate the influence of the mass transfer process on the evolution of the volume fraction. Nonetheless, the rigorous derivation of the pressure-relaxed model (11) from the system (1) reveals that indeed mass transfer terms affect α_k via the pressure relaxation process, as we observe from the contribution of $\mathcal{M}$ appearing in (11a), (11b) (and (15) for the case $N = 2$). Note that neglecting the term $\mathcal{M}/\rho_\mathrm{I}$ in the six-equation two-phase model of [45] does not affect the numerical model and the numerical results presented there, since $\nu = 0$ or $\nu \to +\infty$, and the numerical procedure for treating instantaneous chemical relaxation consists in imposing directly algebraic thermodynamic equilibrium conditions.

3.2. pT-relaxed models

Assuming instantaneous mechanical equilibrium $\mu_{jk} \equiv \mu \to +\infty$ for all the phases and thermal equilibrium $\vartheta_{kj} \equiv \vartheta \to +\infty$ for M phases, $2 \le M \le N$, we obtain a hyperbolic relaxed system of $2N - M + 1 + d$ equations characterized by the speed of sound $c_{pT,M}$, defined by

$$\frac{1}{{c_{pT,M}}^2} = \left(\frac{\partial p}{\partial \rho}\right)_{\sum_{k=1}^{M} Y_k s_k, s_{M+1}, \ldots, s_N, Y_1, \ldots, Y_N}\,, \tag{18}$$

From this definition we obtain the expression:

$$\frac{1}{{c_{pT,M}}^2} = \frac{1}{{c_p}^2} + \frac{\rho T}{\sum_{k=1}^{M} C_{pk}} \sum_{k=1}^{M-1} C_{pk} \sum_{j=k+1}^{M} C_{pj} \left(\frac{\Gamma_j}{\rho_j c_j^2} - \frac{\Gamma_k}{\rho_k c_k^2}\right)^2\,, \tag{19}$$

where T denotes the equilibrium temperature, $C_{pk} = \alpha_k\rho_k\kappa_{pk}$, $\kappa_{pk} = (\partial h_k/\partial T_k)_{p_k}$ (specific heat at constant pressure), and we recall $\Gamma_k = (\partial p_k/\partial \mathcal{E}_k)_{\rho_k}$. Let us note that in the particular case of thermal equilibrium for all the phases, $M = N$, the reduced single-pressure single-temperature pT-relaxed multiphase model has the conservative form:

$$\partial_t(\alpha_1\rho_1) + \nabla\cdot(\alpha_1\rho_1\vec{u}) = \mathcal{M}\,, \tag{20}$$

$$\partial_t(\alpha_2\rho_2) + \nabla\cdot(\alpha_2\rho_2\vec{u}) = -\mathcal{M}\,, \tag{21}$$

$$\partial_t(\alpha_k\rho_k) + \nabla\cdot(\alpha_k\rho_k\vec{u}) = 0\,, \quad k = 3, \ldots, N\,, \tag{22}$$

$$\partial_t(\rho\vec{u}) + \nabla\cdot(\rho\vec{u}\otimes\vec{u} + p\mathbb{I}) = 0\,, \tag{23}$$

$$\partial_t E + \nabla\cdot((E + p)\vec{u}) = 0\,. \tag{24}$$

The two-phase ($N = 2$) version of this model was considered for instance in [37], and more recently in [49].

3.3. pTg-relaxed models

We now assume instantaneous mechanical equilibrium $\mu_{jk} \equiv \mu \to +\infty$ for all the phases, thermal equilibrium $\vartheta_{kj} \equiv \vartheta \to +\infty$ for M phases, $2 \leq M \leq N$, and, additionally, we consider instantaneous chemical relaxation between the liquid and vapor phases 1 and 2, $\nu \to +\infty$. We consider that at least the liquid-vapor phase pair is in thermal equilibrium. With these hypotheses we obtain a hyperbolic relaxed system of $2(N - M + 1) + d$ equations characterized by a speed of sound $c_{pTg,M}$, defined by

$$c_{pTg,M}{}^2 = \left(\frac{\partial p}{\partial \rho}\right)_{\sum_{k=1}^{M} Y_k s_k, s_{M+1}, \ldots, s_N, Y_3, \ldots, Y_N}, \tag{25}$$

from which we obtain

$$\frac{1}{c_{pTg,M}{}^2} = \frac{1}{c_{pT,M}{}^2} + \frac{\rho T}{\sum_{k=1}^{M} C_{pk}} \left(\sum_{k=1}^{M} \frac{\Gamma_k C_{pk}}{\rho_k c_k^2} - \frac{1}{T} \left(\frac{\mathrm{d}T}{\mathrm{d}p}\right)_{\mathrm{sat}} \sum_{k=1}^{M} C_{pk} \right)^2, \tag{26}$$

where we have introduced the derivatives $(\mathrm{d}T/\mathrm{d}p)_{\mathrm{sat}}$ evaluated on the liquid-vapor saturation curve. As expected (cf. *e.g.* [53]), analogously to the two-phase case [18], it is easy to observe from (14), (19), and (26) that sub-characteristic conditions hold, namely the speed of sound of the N-phase mixture is reduced whenever an additional equilibrium assumption is introduced:

$$c_{pTg} \equiv c_{pTg,N} \leq c_{pTg,M}\,, \quad c_{pT} \equiv c_{pT,N} \leq c_{pT,M}\,, \quad \text{and} \quad c_{pTg} < c_{pT} < c_p < c_{\mathrm{f}}\,. \tag{27}$$

Let us note that in the particular case of thermal equilibrium for all the phases, $M = N$, the reduced pTg-relaxed multiphase model corresponds to the well known Homogeneous Equilibrium Model (HEM) [53], composed of the conservation laws for the mixture density ρ, the mixture momentum $\rho\vec{u}$, and the mixture total energy E. The derivation of the expression of the speed of sound for the considered hierarchy of multiphase flow models is detailed in Appendix B. We conclude this section by showing in Figure 1 the behavior of the sound speed for different levels of activation of instantaneous mechanical, thermal and chemical relaxation for a three-phase mixture made of liquid water, water vapor and air (non-condensable gas). Here we plot the speed of sound versus the volume fraction of the total gaseous component $\alpha_{\mathrm{gv}} = \alpha_{\mathrm{v}} + \alpha_{\mathrm{g}}$ for a fixed ratio $\alpha_{\mathrm{g}}/\alpha_{\mathrm{v}} = 0.5$, where here α_{v} is the vapor volume fraction, and α_{g} is the non-condensable gas volume fraction. The reference pressure is $p = 10^5$ Pa, and the reference temperature is the corresponding saturation temperature. The parameters used for the equations of state of the phases are the same as those of the cavitation tube experiment in Section 5.2 (Experiment 5.2.1).

4. Numerical method

We focus now on the numerical approximation of the multiphase system (1), which we can write in compact vectorial form denoting with $q \in \mathbb{R}^{3N-1+d}$ the vector of the unknowns:

$$\partial_t q + \nabla \cdot \mathcal{F}(q) + \varsigma(q, \nabla q) = \psi_\mu(q) + \psi_\vartheta(q) + \psi_\nu(q)\,, \tag{28a}$$

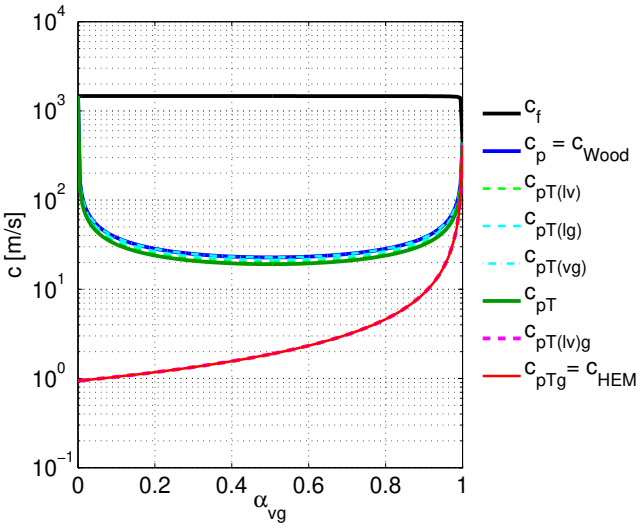

Figure 1: Speed of sound for a three-phase mixture made of liquid water, water vapor and air versus the total gaseous volume fraction $\alpha_{\rm vg} = \alpha_{\rm v} + \alpha_{\rm g}$. We use the subscripts l,v,g to indicate the liquid phase, the vapor phase and the non-condensable gas phase, respectively. $c_{\rm f}$, $c_{pT} = c_{pT,3}$, $c_{pT(jk)} = c_{pT,2}$, $c_{pTg} = c_{pTg,3}$, $c_{pT(jk)g} = c_{pTg,2}$ are the speeds defined in (10), (14), (19), (26). Here the notation $T(jk)$, $j,k = {\rm l,v,g}$, specifies the two phases for which thermal equilibrium is assumed (for instance $c_{pT({\rm lv})}$ denotes the speed of sound for a mixture characterized by pressure equilibrium for all the phases and thermal equilibrium for the liquid and vapor pair only).

$$q = \begin{bmatrix} \alpha_1 \\ \alpha_3 \\ \vdots \\ \alpha_N \\ \alpha_1\rho_1 \\ \alpha_2\rho_2 \\ \vdots \\ \alpha_N\rho_N \\ \rho\vec{u} \\ \alpha_1 E_1 \\ \alpha_2 E_2 \\ \vdots \\ \alpha_N E_N \end{bmatrix}, \quad \mathcal{F}(q) = \begin{bmatrix} 0 \\ 0 \\ \vdots \\ 0 \\ \alpha_1\rho_1\vec{u} \\ \alpha_2\rho_2\vec{u} \\ \vdots \\ \alpha_N\rho_N\vec{u} \\ \rho\vec{u}\otimes\vec{u} + \left(\sum_{k=1}^{N}\alpha_k p_k\right)\mathbb{I} \\ \alpha_1\left(E_1+p_1\right)\vec{u} \\ \alpha_2\left(E_2+p_2\right)\vec{u} \\ \vdots \\ \alpha_N\left(E_N+p_N\right)\vec{u} \end{bmatrix}, \quad \varsigma(q,\nabla q) = \begin{bmatrix} \vec{u}\cdot\nabla\alpha_1 \\ \vec{u}\cdot\nabla\alpha_3 \\ \vdots \\ \vec{u}\cdot\nabla\alpha_N \\ 0 \\ 0 \\ \vdots \\ 0 \\ 0 \\ \Upsilon_1 \\ \Upsilon_2 \\ \vdots \\ \Upsilon_N \end{bmatrix}, \tag{28b}$$

$$\psi_\mu(q) = \begin{bmatrix} \sum_{j=1}^N \mathcal{P}_{1j} \\ \sum_{j=1}^N \mathcal{P}_{3j} \\ \vdots \\ \sum_{j=1}^N \mathcal{P}_{Nj} \\ 0 \\ 0 \\ \vdots \\ 0 \\ 0 \\ -\sum_{j=1}^N p_{I1j}\mathcal{P}_{1j} \\ -\sum_{j=1}^N p_{I2j}\mathcal{P}_{2j} \\ \vdots \\ -\sum_{j=1}^N p_{INj}\mathcal{P}_{Nj} \end{bmatrix}, \quad \psi_\theta(q) = \begin{bmatrix} 0 \\ 0 \\ \vdots \\ 0 \\ 0 \\ 0 \\ \vdots \\ 0 \\ 0 \\ \sum_{j=1}^N \mathcal{Q}_{1j} \\ \sum_{j=1}^N \mathcal{Q}_{2j} \\ \vdots \\ \sum_{j=1}^N \mathcal{Q}_{Nj} \end{bmatrix}, \quad \psi_\nu(q) = \begin{bmatrix} 0 \\ 0 \\ \vdots \\ 0 \\ \mathcal{M} \\ -\mathcal{M} \\ \vdots \\ 0 \\ 0 \\ \left(g_I + \frac{|\vec{u}|^2}{2}\right)\mathcal{M} \\ -\left(g_I + \frac{|\vec{u}|^2}{2}\right)\mathcal{M} \\ \vdots \\ 0 \end{bmatrix}, \tag{28c}$$

with $\Upsilon_k(q, \nabla q)$ defined in (1i). Above we have put into evidence the conservative portion of the spatial derivative contributions in the system as $\nabla \cdot \mathcal{F}(q)$, and we have indicated the non-conservative term as $\varsigma(q, \nabla q)$. The source terms $\psi_\mu(q)$, $\psi_\theta(q)$, $\psi_\nu(q)$ contain mechanical, thermal and chemical relaxation terms, respectively, as expressed in (2).

To numerically solve the system (28) we use the same techniques that we have developed for the two-phase model in [45]. A fractional step method is employed, where we alternate between the solution of the homogeneous system $\partial_t q + \nabla \cdot \mathcal{F}(q) + \varsigma(q, \nabla q) = 0$ and the solution of a sequence of systems of ordinary differential equations (ODEs) that take into account the relaxation source terms ψ_μ, ψ_ϑ, and ψ_ν. As in [45], the resulting method is mixture-energy-consistent, in the sense that (i) it guarantees conservation at the discrete level of the mixture total energy; (ii) it guarantees consistency by construction of the values of the relaxed states with the mixture pressure law. The method has been implemented by using the libraries of the CLAWPACK software [28].

4.1. Solution of the homogeneous system

To solve the hyperbolic homogeneous portion of (28) we employ the wave-propagation algorithms of [30, 29], which are a class of Godunov-type finite volume methods to approximate hyperbolic systems of partial differential equations. We shall consider here for simplicity the one-dimensional case in the x direction ($d = 1$), and we refer the reader to [30] for a comprehensive presentation of these numerical schemes. Hence we consider here the solution of the one dimensional system $\partial_t q + \partial_x f(q) + \varsigma(q, \partial_x q) = 0$, $q \in \mathbb{R}^{3N}$ (as obtained by setting $\vec{u} = u$ and $\nabla = \partial_x$ in (28)). We assume a grid with cells of uniform size Δx, and we denote with Q_i^n the approximate solution of the system at the ith cell and at time t^n, $i \in \mathbb{Z}$, $n \in \mathbb{N}$. The second-order wave propagation algorithm has the form

$$Q_i^{n+1} = Q_i^n - \frac{\Delta t}{\Delta x}(\mathcal{A}^+ \Delta Q_{i-1/2} + \mathcal{A}^- \Delta Q_{i+1/2}) - \frac{\Delta t}{\Delta x}(F^{\mathrm{h}}_{i+1/2} - F^{\mathrm{h}}_{i-1/2})\,. \tag{29}$$

Here $\mathcal{A}^\mp \Delta Q_{i+1/2}$ are the so-called fluctuations arising from Riemann problems at cell interfaces $(i + 1/2)$ between adjacent cells i and $(i + 1)$, and $F^{\mathrm{h}}_{i+1/2}$ are correction terms for (formal) second-order accuracy. To define the fluctuations, a Riemann solver (cf. [20, 55, 30]) must be provided. The solution structure defined by a given solver for a Riemann problem with left and right data

q_ℓ and q_r can be expressed in general by a set of $\mathscr{M}$ waves $\mathcal{W}^l$ and corresponding speeds s^l, $\mathscr{M} \gtreqless 3N$. For example, for the HLLC-type solver described below $\mathscr{M} = 3$. The sum of the waves must be equal to the initial jump in the vector q of the system variables:

$$\Delta q \equiv q_r - q_\ell = \sum_{l=1}^{\mathscr{M}} \mathcal{W}^l. \tag{30}$$

Moreover, for any variable of the model system governed by a conservative equation the initial jump in the associated flux function must be recovered by the sum of waves multiplied by the corresponding speeds. In the considered model the conserved quantities are $\alpha_k\rho_k$, $k = 1, \ldots, N$, and ρu, therefore in order to guarantee conservation we need:

$$\Delta f^{(\xi)} \equiv f^{(\xi)}(q_r) - f^{(\xi)}(q_\ell) = \sum_{l=1}^{\mathscr{M}} s^l \mathcal{W}^{l(\xi)} \tag{31}$$

for $\xi = N, \ldots, 2N$, where $f^{(\xi)}$ is the ξth component of the flux vector f, and $\mathcal{W}^{l(\xi)}$ denotes the ξth component of the lth wave, $l = 1, \ldots, \mathscr{M}$. It is clear that conservation of the partial densities ensures conservation of the mixture density $\rho = \sum_{k=1}^{N} \alpha_k\rho_k$. In addition, we must ensure conservation of the mixture total energy,

$$\Delta f_E \equiv f_E(q_r) - f_E(q_\ell) = \sum_{l=1}^{\mathscr{M}} s^l \sum_{k=1}^{N} \mathcal{W}^{l(2N+k)}, \tag{32}$$

where $f_E = u(E + \sum_{k=1}^{N} \alpha_k p_k)$ is the flux function associated to the mixture total energy E. Once the Riemann solution structure $\{\mathcal{W}^l_{i+1/2}, s^l_{i+1/2}\}_{l=1,\ldots,\mathscr{M}}$ arising at each cell edge $x_{i+1/2}$ is defined through a Riemann solver, the fluctuations $\mathcal{A}^{\mp}\Delta Q_{i+1/2}$ and the higher-order (second-order) correction fluxes $F^{\mathrm{h}}_{i+1/2}$ in (29) are computed as

$$\mathcal{A}^{\pm}\Delta Q_{i+1/2} = \sum_{l=1}^{\mathscr{M}} (s^l_{i+1/2})^{\pm} \mathcal{W}^l_{i+1/2}\,, \tag{33}$$

where we have used the notation $s^+ = \max(s, 0)$, $s^- = \min(s, 0)$, and

$$F^{\mathrm{h}}_{i+1/2} = \frac{1}{2} \sum_{l=1}^{\mathscr{M}} \left|s^l_{i+1/2}\right| \left(1 - \frac{\Delta t}{\Delta x} \left|s^l_{i+1/2}\right|\right) \mathcal{W}^{l\,\mathrm{h}}_{i+1/2}\,, \tag{34}$$

where $\mathcal{W}^{l\,\mathrm{h}}_{i+1/2}$ are a modified version of $\mathcal{W}^l_{i+1/2}$ obtained by applying to $\mathcal{W}^l_{i+1/2}$ a limiter function (cf. [30]).

One difficulty in the solution of the homogeneous portion of the multiphase system (28) is the presence of the non-conservative products Υ_k in the phasic energy equations. Although a discussion of the treatment of non-conservative terms is not the main focus of the present work, it is important to recall the associated issues and challenges. It is well known that a first difficulty of non-conservative hyperbolic systems is the lack of a notion of weak solution in the distributional framework for problems involving shocks. The theory of Dal Maso–LeFloch–Murat [12] has marked an advance by offering a possible definition of weak solution, based on the concept of non-conservative products as a Borel measure associated to a choice of a

family of paths. Even with this rigorous theoretical framework and the assumption of a known correct shock wave solution, further difficulties arise in the design of numerical methods able to correctly approximate non-conservative systems. The path-conservative schemes introduced in the seminal article by Parés [42] are formally consistent with the definition of non-conservative products of [12], once a family of paths has been selected. Nonetheless, this approach has still some known shortcomings as for instance discussed in [9, 1].

Concerning more specifically the multiphase flow model under study with stiff mechanical relaxation, difficulties related to the non-conservative products in the energy equations arise for problems involving shocks in genuine multiphase mixtures (flow conditions not close to nearly single-phase fluids). The shock jump relations for two-phase mixtures in kinetic and mechanical equilibrium derived by Saurel *et al.* in [50] are commonly accepted as the correct shock conditions for the non-conservative pressure equilibrium model (11) (for $N = 2$), since they have been validated over a large set of experimental data (cf. also *e.g.* [46]). These relations allow the construction of an (assumed) exact solution to the pressure equilibrium model in the presence of shocks [47], and hence a solution to the parent multiphase model (1) with instantaneous mechanical relaxation. Even with the knowledge of shock conditions, the design of efficient shock-capturing diffuse-interface numerical methods able to correctly compute shocks in multiphase mixtures is still an open challenge, cf. for instance the methods in [47, 52, 2].

In the present work for the approximation of the non-conservative equations (28) we propose HLLC-type Riemann solvers that are extensions to the multiphase case of the the simple HLLC-type solver illustrated in [45] and of the Suliciu-type solver developed in [15] for the two-phase case. The simple HLLC-type solver of [45] omits the discretization of the non-conservative terms Υ_k in the phasic energy equations. The Suliciu-type solver proposed in [15] can be considered as a generalized HLLC-type method that accounts for the discretization of these non-conservative products. This solver also includes the simple solver of [45] for a special choice of the relaxation parameters. For the two-phase case we have numerically investigated different solvers with different treatments of the non-conservative terms, including the Suliciu-type solver, a Roe-type solver [45, 44, 43], and several path-conservative solvers [15], following in particular the methods in [16, 17]. Typically no relevant differences are observed between results of the various solvers, and results are found to agree with the exact solution of the pressure equilibrium model as constructed in [47], except, as expected, for the case of very strong shocks in genuine multiphase mixture regions, a type of problem which will not be considered in the present work. We refer the reader in particular to [15] for a discussion on this topic.

To conclude this subsection, let us remark that HLLC-type Riemann solvers have gained increased interest in the last decade for applications to multiphase compressible flow models, thanks in particular to the their ability to ensure positivity preservation and entropy conditions, in addition to the advantage of the inherent representation of the intermediate contact wave. A first HLLC-type method for the non-conservative two-phase Baer–Nunziato equations [4] was proposed in [54]. HLLC-type solvers for two-phase flows were also adopted for instance in [52, 63]. Still within the class of extended HLL solvers able to represent intermediate waves, let us finally mention the HLLEM Riemann solver for general conservative and non-conservative hyperbolic systems introduced in [16]. This solver includes the discretization of non-conservative products in the framework of path-conservative HLL schemes and it was applied in [16] to several non-conservative systems, including the Baer–Nunziato equations.

4.1.1. A simple HLLC-type solver

We present in this subsection an extension to the multiphase system (1) of the HLLC-type solver illustrated in [45] for the two-phase case. This solver is obtained by applying the standard HLLC method [56, 55] to the conservative portion of the multiphase system, neglecting the non-conservative terms Υ_k in the phasic energy equations. In the next subsection we will present a generalized HLLC-type solver that takes into account the non-conservative products.

The simple HLLC-type solver consists of three waves $\mathcal{W}^l$, $l = 1, 2, 3$, moving at speeds

$$s^1 = S_\ell\,, \quad s^2 = S^\star\,, \quad \text{and} \quad s^3 = S_r\,, \tag{35}$$

which separate four constant states q_ℓ, $q^{\star\ell}$, $q^{\star r}$ and q_r. In the following we will indicate with $(\cdot)_\ell$ and $(\cdot)_r$ quantities corresponding to the states q_ℓ and q_r, respectively. Moreover, we will indicate with $(\cdot)^{\star\ell}$ and $(\cdot)^{\star r}$ quantities corresponding to the states $q^{\star\ell}$ and $q^{\star r}$ adjacent, respectively on the left and on the right, to the middle wave propagating at speed $S^\star$. With this notation, the waves of the HLLC solver are

$$\mathcal{W}^1 = q^{\star\ell} - q_\ell, \quad \mathcal{W}^2 = q^{\star r} - q^{\star\ell}, \quad \text{and} \quad \mathcal{W}^3 = q_r - q^{\star r}. \tag{36}$$

The middle states $q^{\star\ell}$, $q^{\star r}$ are defined so as to satisfy the following Rankine–Hugoniot conditions, based on the conservative portion of the system:

$$f^{(\xi)}(q^{\star r}) - f^{(\xi)}(q_r) = S_r(q^{\star r(\xi)} - q_r^{(\xi)}), \tag{37a}$$

$$f^{(\xi)}(q_\ell) - f^{(\xi)}(q^{\star\ell}) = S_\ell(q_\ell^{(\xi)} - q^{\star\ell(\xi)}), \tag{37b}$$

$$f^{(\xi)}(q^{\star r})^{(\xi)} - f^{(\xi)}(q^{\star\ell}) = S^\star(q^{\star r(\xi)} - q^{\star\ell(\xi)}), \tag{37c}$$

$\xi = N, \ldots, 3N$. The solution structure for the advected volume fractions α_k simply consists of single jumps $\alpha_{k,r} - \alpha_{k,\ell}$ across the 2-wave moving at speed $S^\star$. Invariance of the equilibrium pressure p and of the normal velocity u is assumed across the 2-wave, in analogy with the exact Riemann solution. Then the speed $S^\star$ is determined as [55]

$$S^\star = \frac{p_r - p_\ell + \rho_\ell u_\ell(S^\ell - u_\ell) - \rho_r u_r(S^r - u_r)}{\rho_\ell(S^\ell - u_\ell) - \rho_r(S^r - u_r)}. \tag{38}$$

A definition for the wave speeds must be provided, see *e.g.* [55, 5]. For the numerical experiments presented in this article we have adopted the following classical simple definition proposed by Davis [14]:

$$S^\ell = \min(u_\ell - c_\ell\,,\, u_r - c_r) \qquad \text{and} \qquad S^r = \max(u_\ell + c_\ell\,,\, u_r + c_r). \tag{39}$$

The middle states are obtained as

$$q^{\star\iota} = \begin{pmatrix} \alpha_{1,\iota} \\ \alpha_{3,\iota} \\ \vdots \\ \alpha_{N,\iota} \\ (\alpha_1\rho_1)_\iota \frac{S_\iota - u_\iota}{S_\iota - S^\star} \\ (\alpha_2\rho_2)_\iota \frac{S_\iota - u_\iota}{S_\iota - S^\star} \\ \vdots \\ (\alpha_N\rho_N)_\iota \frac{S_\iota - u_\iota}{S_\iota - S^\star} \\ \rho_\iota \frac{S_\iota - u_\iota}{S_\iota - S^\star} S^\star \\ (\alpha_1\rho_1)_\iota \frac{S_\iota - u_\iota}{S_\iota - S^\star} \left(\frac{E_{1,\iota}}{\rho_{1,\iota}} + (S^\star - u_\iota)\left(S^\star + \frac{p_{1,\iota}}{\rho_{1,\iota}(S_\iota - u_\iota)}\right)\right) \\ (\alpha_2\rho_2)_\iota \frac{S_\iota - u_\iota}{S_\iota - S^\star} \left(\frac{E_{2,\iota}}{\rho_{2,\iota}} + (S^\star - u_\iota)\left(S^\star + \frac{p_{2,\iota}}{\rho_{2,\iota}(S_\iota - u_\iota)}\right)\right) \\ \vdots \\ (\alpha_N\rho_N)_\iota \frac{S_\iota - u_\iota}{S_\iota - S^\star} \left(\frac{E_{N,\iota}}{\rho_{N,\iota}} + (S^\star - u_\iota)\left(S^\star + \frac{p_{N,\iota}}{\rho_{N,\iota}(S_\iota - u_\iota)}\right)\right) \end{pmatrix}, \tag{40}$$

$\iota = \ell, r$. Note that in the above formulas $p_{k,\iota} = p_\iota$, for all $k = 1, \ldots, N$, since initial Riemann states satisfy pressure equilibrium conditions.

4.1.2. A Suliciu-type solver

We present in this section a Suliciu-type Riemann solver for the multiphase flow model by extending the solver that we have introduced in [15] for the two-phase case. This solver is based on the Suliciu relaxation Riemann solver presented in [8] for the Euler equations. Analogously to the case of the Euler equations, this Suliciu-type solver results to be equivalent to the classical HLLC solver for the discretization of the conservative equations and of the volume fraction equations of the multiphase system. We will show indeed that this solver defines a class of HLLC-type methods that differ for the definition of some constant parameters, which affect the discretization of the non-conservative terms. A particular choice of these parameters gives a Riemann solver exactly equivalent to the simple HLLC-type method described above that neglects nonconservative terms. The Suliciu solver [8] belongs to the class of relaxation Riemann solvers [31], which are based on the idea of approximating the solution of the original system by the solution of an extended system called relaxation system, which is easier to solve. The latter system is assumed to relax to the original one, whose variables define the Maxwellian equilibrium. We refer to [8, 22, 31] for details, and we just present the structure of the relaxation system associated to (1). Let us introduce N auxiliary relaxation variables Π_k, $k = 1, \ldots, N$, which are meant to relax toward the partial pressures, thus at equilibrium $\Pi_k = \alpha_k p_k$, $k = 1, \ldots, N$. The equations governing the partial pressures,

$$\partial_t(\alpha_k p_k) + u\,\partial_x(\alpha_k p_k) + Y_k c_k^2 \rho\,\partial_x u = 0\,, \tag{41}$$

suggest the form of the equations for new variables Π_k, which are independent variables of the relaxation system. We introduce the constant parameters C_k, $k = 1, \ldots, N$, and we replace in the above equations (41) the terms $Y_k c_k^2 \rho^2$ by C_k^2, and $(\alpha_k p_k)$ by Π_k, $k = 1, \ldots, N$. In order to be able to specify different constant C_k for the left and right wave structure of the Riemann problem

solution, we also introduce advection equations for C_k. The Suliciu relaxation system associated to the homogeneous portion of the system (1) in one spatial dimension is:

$$\partial_t \alpha_k + u\partial_x \alpha_k = 0, \quad k = 1, 3, \dots, N, \tag{42a}$$
$$\partial_t(\alpha_k \rho_k) + \partial_x(\alpha_k \rho_k u) = 0, \quad k = 1, \dots, N, \tag{42b}$$
$$\partial_t(\rho u) + \partial_x\left(\rho u^2 + \textstyle\sum_{k=1}^{N} \Pi_k\right) = 0, \tag{42c}$$
$$\partial_t(\alpha_k \rho_k E_k) + \partial_x(\alpha_k \rho_k E_k u + \Pi_k u) + u(Y_k \partial_x\left(\textstyle\sum_{j=1}^{N} \Pi_j\right) - \partial_x \Pi_k) = 0, \quad k = 1, \dots, N, \tag{42d}$$
$$\partial_x \Pi_k + u\partial_x \Pi_k + C_k^2/\rho\, \partial_x u = 0, \quad k = 1, \dots, N, \tag{42e}$$
$$\partial_x C_k + u\partial_x C_k = 0, \quad k = 1, \dots, N. \tag{42f}$$

The eigenvalues of this system are:

$$\tilde{\lambda}_{1,5N} = u \mp \tilde{c}_{\mathrm{m}}\,, \quad \tilde{c}_{\mathrm{m}} = \frac{C_{\mathrm{m}}}{\rho}\,, \quad C_{\mathrm{m}} = \sqrt{\textstyle\sum_{k=1}^{N} C_k^2}\,, \quad \tilde{\lambda}_2 = \dots \tilde{\lambda}_{5N-1} = u\,. \tag{43}$$

All the characteristic fields are linearly degenerate, hence we can easily find the exact solution of the relaxation system through the Riemann invariants. The Suliciu Riemann solver uses this exact solution to approximate the Riemann solution of the original system. The solution structure is analogous to the one of the HLLC solver and it consists of three waves separating four constant states, the left and right states and two middle states adjacent to a discontinuity moving with speed $u^\star$. We will denote quantities corresponding to these middle states with $(\cdot)^{\star\ell}$ adding a subscript $(\cdot)^{\star\ell}_{\mathrm{Sul}}$ if needed to make a distinction with the previous HLLC-type solver.

Riemann invariants. Across the contact discontinuity associated to the eigenvalue u:

$$u = \text{const.}, \quad \Pi_{\mathrm{m}} = \text{const.}, \tag{44}$$

where we have defined $\Pi_{\mathrm{m}} = \sum_{k=1}^{N} \Pi_k$. Across fields associated to the eigenvalues $u \mp \tilde{c}_{\mathrm{m}}$:

$$\alpha_k, Y_k = \text{const.}, \quad k = 1, \dots, N, \tag{45a}$$
$$\frac{1}{\rho} + \frac{\Pi_k}{C_k^2} = \text{const.}, \quad k = 1, \dots, N, \tag{45b}$$
$$u \mp \tilde{c}_{\mathrm{m}} = \text{const.}, \tag{45c}$$
$$C_k^2 \Pi_j - C_j^2 \Pi_k = \text{const.}, \quad k, j = 1, \dots, N, \tag{45d}$$
$$Y_k \varepsilon_k - \frac{\Pi_k^2}{2C_k^2} = \text{const.}, \quad k = 1, \dots, N, \tag{45e}$$
$$C_k = \text{const.}, \quad k = 1, \dots, N. \tag{45f}$$

By using (45b) and (45c) we also deduce:

$$\Pi_k \pm \frac{C_k^2}{C_{\mathrm{m}}} u = \text{const.}, \quad k = 1, \dots, N, \tag{46}$$

and by using (45d) and (45b):

$$\frac{1}{\rho} + \frac{\Pi_{\mathrm{m}}}{C_{\mathrm{m}}^2} = \text{const.}. \tag{47}$$

Then, by using (46), we infer:

$$\Pi_{\mathrm{m}} \pm C_{\mathrm{m}} u = \text{const.}\,. \tag{48}$$

Let us note first that $(\Pi_k)_{\ell,r} = (\alpha_k p_k)_{\ell,r}$, and $(\Pi_{\mathrm{m}})_{\ell,r} = (p_{\mathrm{m}})_{\ell,r}$, where $p_{\mathrm{m}} = \sum_{k=1}^{N} \alpha_k p_k$. Moreover, since initial Riemann states are characterized by pressure equilibrium, we can write $p_{\mathrm{m}\ell} = p_\ell$ and $p_{\mathrm{m}r} = p_r$. The relations (44) and (48) determine the quantities $u^{\star\ell}_{\mathrm{Sul}} = u^{\star r}_{\mathrm{Sul}} \equiv u^\star$ and $(\Pi_{\mathrm{m}})^{\star\ell} = (\Pi_{\mathrm{m}})^{\star r} \equiv \Pi^\star_{\mathrm{m}}$:

$$u^\star = \frac{\rho_\ell \tilde{c}_{\mathrm{m}\ell} u_\ell + \rho_r \tilde{c}_{\mathrm{m}r} u_r + p_\ell - p_r}{\rho_\ell \tilde{c}_{\mathrm{m}\ell} + \rho_r \tilde{c}_{\mathrm{m}r}}, \quad \Pi^\star_{\mathrm{m}} = \frac{\rho_\ell \tilde{c}_{\mathrm{m}\ell} p_\ell + \rho_r \tilde{c}_{\mathrm{m}r} p_r - \tilde{c}_{\mathrm{m}\ell}\tilde{c}_{\mathrm{m}r}(u_r - u_\ell)}{\rho_\ell \tilde{c}_{\mathrm{m}\ell} + \rho_r \tilde{c}_{\mathrm{m}r}}. \tag{49}$$

The expression (47) determines $\rho^{\star\ell,r}_{\mathrm{Sul}}$:

$$\rho^{\star\ell,r}_{\mathrm{Sul}} = \left(\frac{1}{\rho_{\ell,r}} + \frac{c_{r,\ell}(u_r - u_\ell) \mp (p_r - p_\ell)}{c_{\ell,r}(c_\ell + c_r)} \right)^{-1}, \tag{50}$$

and through (45a) we can determine $(\rho_k)^{\star\ell,r}_{\mathrm{Sul}} = (Y_k)_{\ell,r} \rho^{\star\ell,r}_{\mathrm{Sul}} / (\alpha_k)_{\ell,r}$. Then we can find through (46):

$$(\Pi_k)^{\star\ell,r} = (\Pi_k)_{\ell,r} + \frac{(C_k)^2_{\ell,r}}{(C^2_{\mathrm{m}})_{\ell,r}} (\Pi^\star_{\mathrm{m}} - p_{\ell,r}), \quad k = 1, \ldots, N. \tag{51}$$

Finally (45e) determines the specific phasic internal energies $(\varepsilon_k)^{\star\ell,r}_{\mathrm{Sul}}$. Then the intermediate states for the partial phasic energies per unit volume can be expressed as:

$$(\alpha_k \rho_k \varepsilon_k)^{\star\ell,r}_{\mathrm{Sul}} = (\alpha_k \rho_k)^{\star\ell,r}_{\mathrm{Sul}} (\varepsilon_k)_{\ell,r} + \rho^{\star\ell,r}_{\mathrm{Sul}} \left(\frac{(C^2_k)_{\ell,r}}{2((C^2_{\mathrm{m}})_{\ell,r})^2} (\Pi^\star_{\mathrm{m}} - p_{\ell,r})^2 + \frac{(\Pi_k)_{\ell,r}}{(C^2_{\mathrm{m}})_{\ell,r}} (\Pi^\star_{\mathrm{m}} - p_{\ell,r}) \right), \tag{52}$$

and the corresponding total energies are $(\alpha_k E_k)^{\star\ell,r}_{\mathrm{Sul}} = (\alpha_k \rho_k \varepsilon_k)^{\star\ell,r}_{\mathrm{Sul}} + (\alpha_k \rho_k)^{\star\ell,r}_{\mathrm{Sul}} \frac{u^{\star 2}}{2}$. Let us also note that by using (45d) and (45e) we obtain for the mixture specific internal energy $\varepsilon = \sum_{k=1}^{N} Y_k \varepsilon_k$ the invariant:

$$\varepsilon - \frac{\Pi^2_{\mathrm{m}}}{2C^2_{\mathrm{m}}} = \text{const.}\,. \tag{53}$$

Having now the intermediate states, the waves of the Suliciu-type solver are obtained as:

$$\mathcal{W}^1 = q^{\star\ell}_{\mathrm{Sul}} - q_\ell\,, \quad \mathcal{W}^2 = q^{\star r}_{\mathrm{Sul}} - q^{\star\ell}_{\mathrm{Sul}}\,, \quad \text{and} \quad \mathcal{W}^3 = q_r - q^{\star r}_{\mathrm{Sul}}\,. \tag{54}$$

and the corresponding speeds are:

$$s^1 = u_\ell - \tilde{c}_{\mathrm{m}\ell}\,, \quad s^2 = u^\star\,, \quad \text{and} \quad s^3 = u_r + \tilde{c}_{\mathrm{m}r}\,. \tag{55}$$

We observe that the expressions of the invariants (44), (47), (48) and (53) are identical to those of the Suliciu solver for the Euler equations with now Π_{m} and C_{m} playing the role of the relaxation variable associated to the pressure p and the constant $C = \rho c$ of the single-phase case, respectively. Therefore the solution for the intermediate states $(\cdot)^{\star\ell,r}$ of the mixture quantities of the multiphase solver has the same form of the solution for the intermediate states of the standard single-phase Suliciu solver (see formulas in Bouchut's book [8]). It follows that $u^\star = S^\star$ and the intermediate states for α_k and the conserved quantities (partial densities, mixture momentum, mixture total energy) are identical to those of the simple HLLC solver presented in the previous

subsection, $q^{\star\ell,r(\xi)}_{\text{Sul}} = q^{\star\ell,r(\xi)}$, with $q^{\star\ell,r}$ given in (40), for the components $\xi = 1,\dots,2N$, as long as

$$S_\ell = u_\ell - \tilde{c}_{\text{m}\ell} \quad \text{and} \quad S_r = u_r + \tilde{c}_{\text{m}r}\,. \tag{56}$$

Note that the intermediate states for the conserved quantities depend merely on the sum $C^2_{\text{m}} = \sum_{k=1}^N C_k^2$, and only the intermediate states for the phasic energies depend on the individual parameters C_k. The choice of $C_k\,,\ k = 1,\dots,N$, for a given definition of C_{m} defines the partition of the phasic energies within the mixture, based on the invariant (45d).

Choice of parameters. The parameters C_k need to be chosen so that Liu's subcharacteristic condition [35] holds:

$$\tilde{c}_{\text{m}} = \frac{\sqrt{\sum_{k=1}^N C_k^2}}{\rho} \geq c_{\text{f}}\,, \tag{57}$$

where c_{f} is the *frozen* speed of sound defined in (10). Hence the simplest less dissipative definition for the parameters of the local right and left states would be $(C_k^2)_{\ell,r} = (Y_k c_k^2 \rho^2)_{\ell,r}$, which implies $(\tilde{c}_{\text{m}})_{\ell,r} = (c_{\text{f}})_{\ell,r}$. However, this definition is not suitable when shocks are involved in the solution structure. The idea here is to consider well known robust definitions of the wave speeds used for the HLLC solver to define first $\tilde{c}_{\text{m}}$ and then C_k. To begin with, let us propose a definition corresponding to the Davis' wave speeds in (39). We set:

$$\tilde{c}_{\text{m}\ell} = \max(c_{\text{f}\ell}\,,(c_{\text{f}r} + u_\ell - u_r))\,, \quad \tilde{c}_{\text{m}r} = \max(c_{\text{f}r}\,,(c_{\text{f}\ell} + u_\ell - u_r))\,, \tag{58}$$

and we define C_k as:

$$(C_k^2)_{\ell,r} = (Y_k\,\tilde{c}_k^2\,\rho^2)_{\ell,r}, \quad k = 1,\dots,N, \tag{59a}$$

where

$$(\tilde{c}_k)^2_{\ell,r} = \begin{cases} (c_k)^2_{\ell,r} & \text{if} \quad (c_{\text{f}})_{\ell,r} \geq (c_{\text{f}})_{r,\ell} + u_\ell - u_r\,, \\ (c_k)^2_{r,\ell} + 2(u_\ell - u_r)(c_{\text{f}})_{r,\ell} + (u_\ell - u_r)^2 & \text{otherwise.} \end{cases} \tag{59b}$$

Another possible definition of the wave speeds is the one proposed by Bouchut for the single-phase Suliciu solver [8]. We define:

$$(\tilde{c}_{\text{m}})_{\ell,r} = (c_{\text{f}})_{\ell,r} + X_{\ell,r}\,, \tag{60a}$$

where

$$\text{if } p_r - p_\ell \geq 0: \begin{cases} X_\ell = \beta\left(\frac{p_r - p_\ell}{\rho_r c_{\text{f}r}} + u_\ell - u_r\right)^+ \\ X_r = \beta\left(\frac{p_\ell - p_r}{\rho_\ell \tilde{c}_{\text{m}\ell}} + u_\ell - u_r\right)^+ \end{cases}, \text{ if } p_r - p_\ell \leq 0: \begin{cases} X_r = \beta\left(\frac{p_\ell - p_r}{\rho_\ell c_{\text{f}\ell}} + u_\ell - u_r\right)^+ \\ X_\ell = \beta\left(\frac{p_r - p_\ell}{\rho_r \tilde{c}_{\text{m}r}} + u_\ell - u_r\right)^+ \end{cases}. \tag{60b}$$

Then we set:

$$(C_k^2)_{\ell,r} = (Y_k)_{\ell,r}((c_k^2)_{\ell,r} + X^2_{\ell,r} + 2X_{\ell,r}(c_{\text{f}})_{\ell,r})\rho^2_{\ell,r}\,. \tag{61}$$

This choice of the wave speeds allows us to rigorously guarantee positivity preservation for the partial densities and the mixture internal energy, as long as the constant $\beta \geq 1$ satisfies [8]:

$$\frac{\partial}{\partial\rho}\left(\rho\sqrt{\frac{\partial p_{\text{m}}(\rho, s_k, s_N, \alpha_k, Y_k)_{k=1,\dots,N-1}}{\partial\rho}}\right) \leq \beta\sqrt{\frac{\partial p_{\text{m}}(\rho, s_k, s_N, \alpha_k, Y_k)_{k=1,\dots,N-1}}{\partial\rho}}\,. \tag{62}$$

Assuming a stiffened gas equation of state for each phase, we can satisfy the condition above by defining $\beta = \frac{\max_k \gamma_k + 1}{2}$. Let us recall that α_k, as well as Y_k, are governed by advection equations, hence positivity is preserved also for these variables. Moreover, since, as we have noted above, only the intermediate states of the phasic energies depend on the individual parameters C_k, if negative phasic energies are found for the intermediate states (see (45e)), we can always redefine $(C_k)_{\ell,r}$ in order to preserve positivity, still keeping the same values $(C_{\rm m})_{\ell,r}$. Let us finally remark that, given a definition of $C_{\rm m}$, if we define

$$(C_k^2)_{\ell,r} = (Y_k C_{\rm m}^2)_{\ell,r} \tag{63}$$

then the resulting Suliciu-type solver is entirely equivalent to the simple HLLC-type solver described in the previous subsection, which neglects the discretization of the nonconservative terms in the phasic energy equations of the system (1). We can also estimate the difference of the wave components for the phasic energies for the case of the new Suliciu/HLLC-type solver based on a given definition of C_k and the previous simple HLLC-type solver based on (63):

$$(\alpha_k \rho_k E_k)^{\star\ell,r}_{\rm Sul} = (\alpha_k \rho_k E_k)^{\star\ell,r}_{\rm HLLC} + \Delta(\alpha_k \rho_k E_k)^{\star\ell,r}, \tag{64}$$

with

$$\Delta(\alpha_k \rho_k E_k)^{\star\ell,r} = \frac{\rho^\star_{\ell,r}}{2(C_{\rm m}^2)_{\ell,r}} (\Pi^\star - p_{\ell,r})^2 \left(\frac{(C_k^2)_{\ell,r}}{(C_{\rm m}^2)_{\ell,r}} - (Y_k)_{\ell,r} \right). \tag{65}$$

4.2. Relaxation steps

After solving the homogeneous system, we solve a sequence of ordinary differential equations accounting for the relaxation source terms of (1). Here we assume that the characteristic time for mechanical relaxation is much smaller than the characteristic time scales for heat and mass transfer (cf. for instance [23]), and we consider that thermal and chemical relaxation occur under pressure equilibrium. The steps are the following, using here the vector notation in (28):

1. Mechanical relaxation. We solve in the limit $\mu_{kj} \equiv \mu \to +\infty$ the system of ODEs:

$$\partial_t q = \psi_\mu(q). \tag{66}$$

   This step drives instantaneously the flow to pressure equilibrium, $p_k = p$, for all k.

2. Thermal relaxation. We solve in the limit $\mu \to +\infty$, $\vartheta_{kj} \to +\infty$:

$$\partial_t q = \psi_\mu(q) + \psi_\vartheta(q). \tag{67}$$

   This step drives the chosen phase pairs (k, j) to thermal equilibrium, while maintaining pressure equilibrium.

3. Chemical relaxation. We solve in the limit $\mu \to +\infty$, $\vartheta_{kj} \to +\infty$, and $\nu \to +\infty$:

$$\partial_t q = \psi_\mu(q) + \psi_\vartheta(q) + \psi_\nu(q). \tag{68}$$

In the steps 2-3 thermal relaxation can be activated for a subset of phase pairs (k, j), however it is always activated for the phases of the species that may undergo phase transition if chemical relaxation (step 3) is also activated. Thermal and chemical relaxation processes are typically activated at interfaces only. Similar to [27, 45], the numerical relaxation procedures to handle infinitely fast transfer processes are based on the idea of imposing directly equilibrium conditions to obtain a simple system of algebraic equations to be solved in each relaxation step, as we detail below.

4.2.1. Mechanical Relaxation

We consider the solution of the system (66) in the limit $\mu \to +\infty$. We denote with superscript 0 the quantities at initial time, which come from the solution of the homogeneous system, and with superscript $*$ the quantities at final time, which are the quantities at mechanical equilibrium. First, we easily see that the exact solution of the system of ODEs gives $(\alpha_k\rho_k)^* = (\alpha_k\rho_k)^0$, $k = 1, \dots, N$, and $(\rho\vec{u})^* = (\rho\vec{u})^0$, $E^* = E^0$, hence $\vec{u}^* = \vec{u}^0$ and $\mathcal{E}^* = \mathcal{E}^0$. We then integrate the equations for the phasic total energies by approximating the interface pressures p_{Ikj} with their values at equilibrium $p^*_{Ikj} = p^*$. We then obtain N equations of the form

$$(\alpha_k E_k)^* - (\alpha_k E_k)^0 = (\alpha_k \mathcal{E}_k)^* - (\alpha_k \mathcal{E}_k)^0 = -p^*(\alpha_k^* - \alpha_k^0) \tag{69}$$

for $k = 1, 2, \dots, N$. Imposing the pressure equilibrium conditions $p_k = p^*$, for all $k = 1, \dots, N$, at final time the phasic internal energies are then expressed as $\mathcal{E}_k^* = \mathcal{E}_k(p^*, (\alpha_k\rho_k)^0/\alpha_k^*)$. With these relations the system (69) and the constraint $\sum_{k=1}^N \alpha_k = 1$ give $N + 1$ equations for the unknowns α_k^*, $k = 1, \dots, N$, and p^*. For the particular case of the SG EOS (3) the problem can be reduced to the solution of a polynomial equation of degree N for the equilibrium pressure p^*. In general an iterative solution procedure is needed to solve this equation. Let us remark that for the most part of the three-phase ($N = 3$) flow numerical tests considered in this work we have two gaseous phases governed by a SG EOS with $\varpi_k = 0$. In this particular case the polynomial equation of degree 3 for p^* reduces to a quadratic equation, whose physically admissible solution is easily found.

4.2.2. Thermal Relaxation

If thermal relaxation terms are also activated, then we consider the solution of the system (67), with $\mu_{kj} \equiv \mu \to +\infty$ for all phase pairs, and $\vartheta_{kj} \equiv \vartheta \to +\infty$ for some desired pairs (k, j). Let us assume instantaneous thermal equilibrium for M phases, $2 \le M \le N$, in addition to mechanical equilibrium for all phases. We will denote equilibrium values with the superscript $**$. Then, analogously to the case of pressure relaxation, we can write $(\alpha_k\rho_k)^{**} = (\alpha_k\rho_k)^0$, $k = 1, \dots, N$, $(\rho\vec{u})^{**} = (\rho\vec{u})^0$, $E^{**} = E^0$, and $\mathcal{E}^{**} = \mathcal{E}^0$. Moreover, we write $N - M$ equations of the form (69) with $(\cdot)^0$ replaced by $(\cdot)^*$ and $(\cdot)^*$ replaced by $(\cdot)^{**}$, the mechanical equilibrium conditions $p_k^{**} = p^{**}$, for all $k = 1, \dots, N$, and the thermal equilibrium conditions $T_k^{**} = T^{**}$ for M phases. All these relations give a system of algebraic equations to be solved for the equilibrium values α_k^{**}, p^{**}. As for the mechanical relaxation step, the solution of this system of algebraic equations can be reduced to the solution of a polynomial equation of degree N for the pressure p^{**} when the SG EOS is adopted. The problem reduces further to the solution of a quadratic equation for the case $N = 3$ with two gaseous phases governed by SG pressure laws with $\varpi_k = 0$.

4.2.3. Thermo-Chemical Relaxation

If thermo-chemical relaxation is activated for the species that may undergo liquid/vapor transition, then we solve the system of ODEs (68) with $\mu_{kj} \equiv \mu \to +\infty$ for all phase pairs, $\vartheta_{kj} \equiv \vartheta \to +\infty$ for some phase pairs (k, j), and $\nu \to +\infty$ for the phase pair $(1, 2)$. Let us assume instantaneous thermal equilibrium for M phases, including at least the phases 1 and 2. We denote the quantities at thermodynamic equilibrium with the superscript $\oplus$. First, we can write $\rho^\oplus = \rho^0$, $(\rho\vec{u})^\oplus = (\rho\vec{u})^0$, $E^\oplus = E^0$, and $\mathcal{E}^\oplus = \mathcal{E}^0$. Moreover, we write $N - M$ equations of the form (69) with $(\cdot)^0$ replaced by $(\cdot)^{**}$ and $(\cdot)^*$ replaced by $(\cdot)^\oplus$, the mechanical equilibrium conditions $p_k^\oplus = p^\oplus$, for all $k = 1, \dots, N$, the thermal equilibrium conditions $T_k^\oplus = T^\oplus$ for M

phases, and the chemical equilibrium condition $g_1^{\oplus} = g_2^{\oplus}$. This set of algebraic equations can be solved for the values of the equilibrium pressure $p^{\oplus}$, the equilibrium volume fractions $\alpha_k^{\oplus}$ and the equilibrium densities $\rho_k^{\oplus}$. For the case of three-phase flow with SG EOS considered here we use a solution procedure similar to the two-phase case [45]. First we reduce the set of algebraic conditions excluding the chemical equilibrium relation to the solution of a quadratic equation for the temperature as a function of the equilibrium pressure, $T^{\oplus} = T^{\oplus}(p^{\oplus})$. Then the expression of $T^{\oplus}(p^{\oplus})$ is introduced into the equilibrium condition $g_1^{\oplus} = g_2^{\oplus}$. This gives an equation for $p^{\oplus}$, which is solved by Newton's iterative method. Let us remark that a physically admissible solution of system (68) might not exist. In such a case we use the same technique that we have proposed in [45] (p. 356): we consider that the species that may undergo transition consists almost entirely of the phase (liquid or vapor) that has higher entropy, hence we fix the volume fraction of the negligible phase to a small tolerance (for instance = 10^{-8}), and this new equation for one volume fraction replaces the equation $g_1^{\oplus} = g_2^{\oplus}$ in the algebraic system that we have defined with pressure and temperature equilibrium conditions. Among the admissible solutions of this new system we select the solution that maximizes the total entropy. Note that again the problem reduces further to the solution of a quadratic equation for the case $N = 3$ with two gaseous phases governed by SG pressure laws with $\varpi_k = 0$, as in the experiments with phase transition considered here.

5. Numerical experiments

We present in this section numerical results for test problems involving three-phase flows ($N = 3$). All the computations have been performed with the second-order wave propagation algorithm with the simple HLLC-type solver described in Section 4.1.1. We report results obtained with the generalized HLLC-type Riemann solver described in Section 4.1.2 based on the Suliciu relaxation system only for the first two one-dimensional experiments since for the set of tests considered in this work no relevant differences are observed between the two solvers.

5.1. Test problems with no phase transition

To begin with, we consider test problems without mass transfer processes (no chemical relaxation step).

Experiment 5.1.1. Our first numerical example concerns a three-phase flow problem simulated by Billaud Friess and Kokh [7] by an extended multicomponent formulation of the two-phase transport five-equation model presented previously in [3]. Our aim here is to verify that our computed solution is an accurate approximation of the exact solution of the multiphase flow model with instantaneous pressure relaxation. This test involves three fluid phases in mechanical equilibrium in a one-dimensional domain $[0, 1]$ m. The phases are all modeled by the ideal polytropic gas law with the ratio of the specific heats defined by $\gamma_1 = 1.6$, $\gamma_2 = 2.4$, and $\gamma_3 = 1.4$. Initially, the velocity is zero, and the phasic densities are $\rho_1 = 1$ kg/m^3, $\rho_2 = 0.125$ kg/m^3, and $\rho_3 = 0.1$ kg/m^3 in the entire domain. There are two initial discontinuities located at $x = 0.4$ m and $x = 0.6$ m that separate the domain into three parts with the remaining state variables in each region set as

$$(p, \alpha_1, \alpha_2) = \begin{cases} \left(1\,\text{Pa}, 1 - 2 \cdot 10^{-6}, 10^{-6}\right) & \text{if } x \in [0, 0.4)\ \text{m}, \\ \left(0.1\,\text{Pa}, 10^{-6}, 1 - 2 \cdot 10^{-6}\right) & \text{if } x \in [0.4, 0.6)\ \text{m}, \\ \left(0.1\,\text{Pa}, 10^{-6}, 10^{-6}\right) & \text{if } x \in [0.6, 1]\ \text{m}. \end{cases}$$

Table 1: Equation of state parameters employed in the Experiment 5.1.2.

k (phase)	γ	ϖ [MPa]	η [kJ/kg]	η' [kJ/(Kg · K)]	κ_v [J/(kg · K)]
1 (carbon dioxide)	1.03	13.47	0	0	3764
2 (water)	2.85	833.02	0	0	1458
3 (methane)	1.23	10.94	0	0	2382

Figure 2 shows the density contours of the exact solution of the three-phase pressure equilibrium model for this problem in the x-t plane up to time $t = 0.14$ s. This exact solution has been computed based on the algorithm described in [47]. From the graph, it is easy to see that the initial discontinuity at $x = 0.4$ m originates a leftward-going rarefaction wave, a rightward-going contact discontinuity, and a shock wave. As time progresses, the shock wave moves toward the material interface at $x = 0.6$ m, and then collides, yielding a new set of waves from the collision. Further collisions then occur. We compute the numerical solution for this test by employing both the simple HLLC-type solver described in Section 4.1.1, and the Suliciu-type solver (generalized HLLC-type solver) presented in Section 4.1.2. We use 1000 grid cells, Courant number = 0.5, and we apply second-order corrections with the minmod limiter. Numerical results are displayed in Fig. 3, together with the exact solution for this problem. We observe that results obtained by the HLLC-type solver and by the Suliciu-type solver are not distinguishable, and they both agree well with the exact solution. Let us also remark that for this test problems, and more generally for multifluid problems involving defined interfaces between nearly pure inert phases, solutions to the multiphase pressure-equilibrium model (11) are similar to solutions to the multicomponent extended five-equation model of [7]. Hence our results here are similar to those in [7]. Let us remark however that the five-equation model of [7] cannot describe cavitation processes. We refer the reader to [41] for some comparison between the five-equation transport model [3] and the five-equation pressure-equilibrium Kapila *et al.* [23] model.

Experiment 5.1.2. We now consider a three-phase (CO_2-water-methane) flow problem simulated by Morin *et al.* [40], where an extended four-equation model is used for the numerical approximation. Here the three fluid components are assumed to be both in mechanical and thermal equilibrium. Hence this test gives us an example to verify our algorithm with the activation of both the mechanical and the thermal relaxation procedure. Initially, the temperature is uniform and equal to $T = 310$ K throughout the domain, corresponding to the interval $[0, 1]$ m. We set the pressure $p = 1.5$ MPa and the velocity $u = 12$ m/s in a region where $x \in [0, 0.5]$ m, and $p = 0.9$ MPa, $u = 0$ m/s in a region where $x \in [0.5, 1]$ m. With these data the phasic density ρ_k, $k = 1, 2, 3$, can be written as a function of p and T in each region, by using (3b) with the material-dependent parameters shown in Table 1. Here a uniform composition of the media is used with volume fractions $\alpha_1 = 0.9$, $\alpha_2 = 0.04$, and $\alpha_3 = 0.06$ in each portion of the domain.

Second-order numerical results obtained by using the HLLC-type solver and the Suliciu-type solver with 1000 grid cells and Courant number = 0.5 are shown in Fig. 4 at time $t = 1.6$ ms. The exact solution of this problem is also displayed for comparison. It is easy to observe that our computed solutions are in good agreement with the exact solution, composed of a leftward-going rarefaction wave, a rightward-going contact discontinuity and a rightward-going shock wave. Again, results obtained with the HLLC-type scheme and with the Suliciu-type scheme overlap. We note that the exact solution computed here is based on the algorithm proposed in [47] for a mechanical equilibrium flow with a modification to include the thermal equilibrium condition in the iterative step of the method.

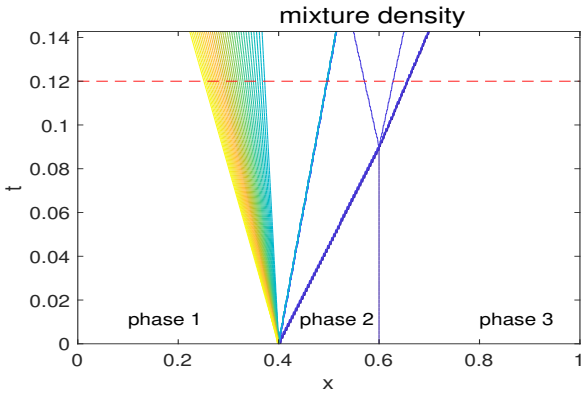

Figure 2: Exact solution for a mechanical equilibrium three-phase shock tube problem; the density contour plot in the x-t plane is shown. The horizontal red dashed line plotted in the graph corresponds to the time $t = 0.12$ s of the snapshots of the solution shown in Fig. 3.

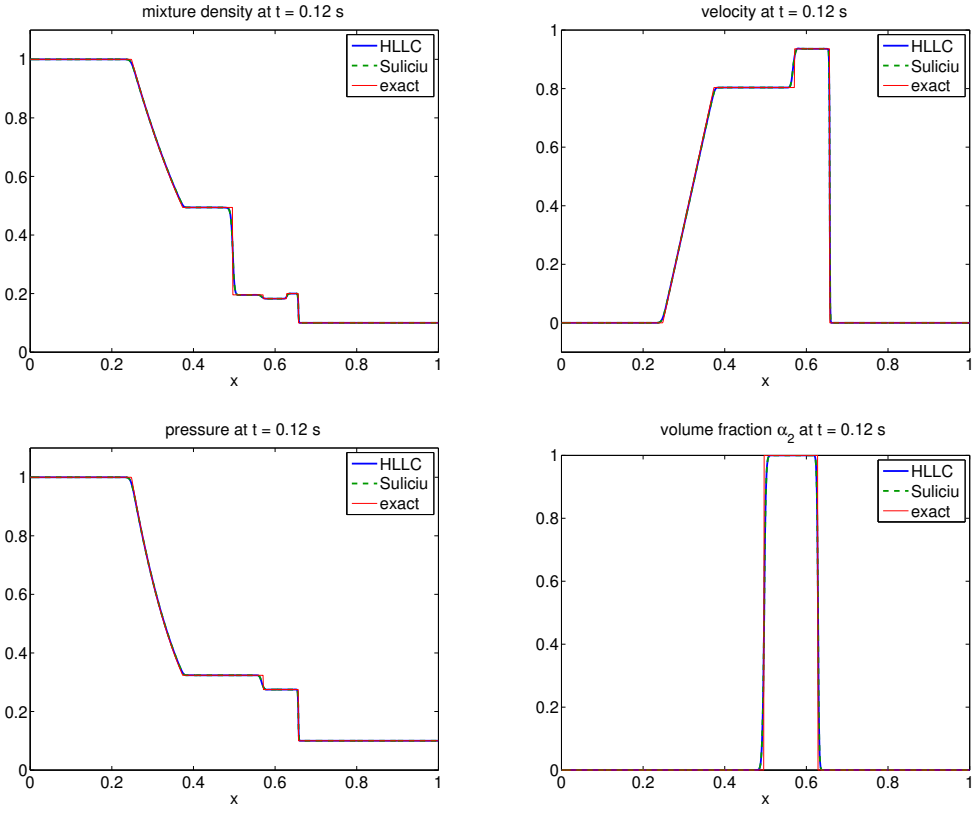

Figure 3: Second-order results for the three-phase shock tube problem (Experiment 5.1.1). From left to right and from top to bottom: mixture density, velocity, pressure and volume fraction α_2 at time $t = 0.12$ s obtained with the HLLC-type solver (solid blue line) and the Suliciu-type solver (dashed green line). Results computed with the two solvers overlap. The thin solid red line indicates the exact solution.

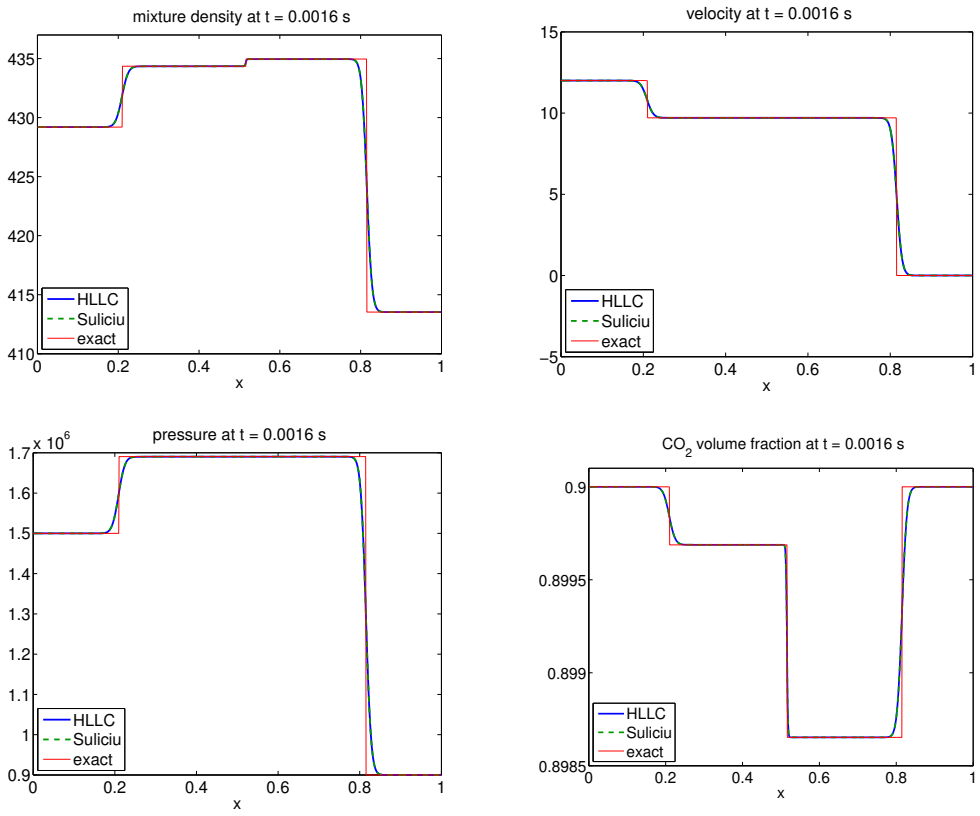

Figure 4: Second-order results for the three-phase CO_2-water-methane Riemann problem (Experiment 5.1.2). From left to right and from top to bottom: mixture density, velocity, pressure and volume fraction at time $t = 0.16$ ms obtained with the HLLC-type solver (solid blue line) and the Suliciu-type solver (dashed green line). Results computed with the two solvers overlap. The thin solid red line indicates the exact solution.

Experiment 5.1.3. As a first test problem in two dimensions, we are interested in a three-phase (air-R22-He) shock-bubble interaction problem studied numerically by Billaud Friess and Kokh [7]. The domain is a closed tube $[0, 445] \times [0, 89]\,\mathrm{mm}^2$, and solid wall boundary conditions are imposed on all the four sides. We set a leftward-going planar Mach 1.22 shock wave in air initially located at $x = 275$ mm, traveling toward a stationary cylindrical Helium bubble with a R22 shell surrounding it. Here the radius of the Helium bubble is $r_0 = 15$ mm, centered at $(x_0, y_0) = (225, 0)$ mm, and the thickness of the R22 cylindrical shell is $H_0 = 10$ mm. We assume that all the fluid phases, *i.e.*, air, R22 (Chlorodifluoromethane), and Helium, are modeled by the ideal polytropic gas law and we set $(\gamma, \rho_0)_1 = (1.4, 1.225\,\mathrm{kg/m}^3)$, $(\gamma, \rho_0)_2 = (1.249, 3.863\,\mathrm{kg/m}^3)$, and $(\gamma, \rho_0)_3 = (1.6, 0.138\,\mathrm{kg/m}^3)$, respectively. The state variables in the region ahead of the shock wave are assumed to correspond to atmospheric condition with pressure $p_0 = 1.01325 \times 10^5$ Pa, and inside the R22-Helium bubble with $r^2 = (x - x_0)^2 + (y - y_0)^2$ and $r_1 = r_0 + H_0$, we set

$$(\rho_1, \rho_2, \rho_3, p, \alpha_1, \alpha_2) = \begin{cases} \left(\rho_{01}, \rho_{02}, \rho_{03}, p_0, 10^{-8}, 10^{-8}\right) & \text{if } r < r_0, \\ \left(\rho_{01}, \rho_{02}, \rho_{03}, p_0, 10^{-8}, 1 - 2 \cdot 10^{-8}\right) & \text{if } r_0 \le r < r_1, \end{cases}$$

while outside the bubble we have

$$(\rho_1, \rho_2, \rho_3, p, \alpha_1, \alpha_2) = \left(\rho_{01}, \rho_{02}, \rho_{03}, p_0, 1 - 2 \cdot 10^{-8}, 10^{-8}\right).$$

Behind the shock, we set

$$\begin{aligned} &(\rho_1, \rho_2, \rho_3, u, v, p, \alpha_1, \alpha_2) \\ &\qquad = \left(1.686\,\mathrm{kg/m}^3, \rho_{02}, \rho_{03}, -113.5\,\mathrm{m/s}, 0, 1.59 \times 10^5\,\mathrm{Pa}, 1 - 2 \cdot 10^{-8}, 10^{-8}\right). \end{aligned}$$

Figure 5 shows pseudo-color plots of the density at six different times $t = 0$, 120, 480, 780, $1020\,\mu$s obtained by using the second-order HLLC-type wave propagation method with instantaneous pressure relaxation on a 1250×250 mesh. Comparing our numerical solution results with those reported in [7] (cf. Fig. 20 in particular), we observe qualitatively good agreement on the geometric structure of the R22-Helium bubble at times up to $t = 480\,\mu$s. At the other times $t = 780$ and $1020\,\mu$s noticeable differences can be seen on the outer ring of the Helium bubble, which consists mostly of the phase of R22. We expect that these visible differences in the results are not related to the differences in the underlying flow models, as we mentioned above. To verify our solution, we have performed the same test by employing a numerical model based on the multicomponent extended five-equation model (cf. [7]) in the simulation. Numerical results of this run are presented in Fig. 6 at three different times $t = 480$, 780, and $1020\,\mu$s. Agreement of the these numerical results with those shown in Fig. 5 can be easily observed.

5.2. Test problems with phase transition

We now present several numerical experiments involving phase transition. For these tests we activate chemical relaxation.

Experiment 5.2.1. We perform a test that is similar to the two-phase cavitation tube experiment presented in [51, 45]. We consider a tube filled initially with liquid water with a uniformly distributed small amount of water vapor with volume fraction $\alpha_{\mathrm{wv}} = 10^{-2}$, and a small

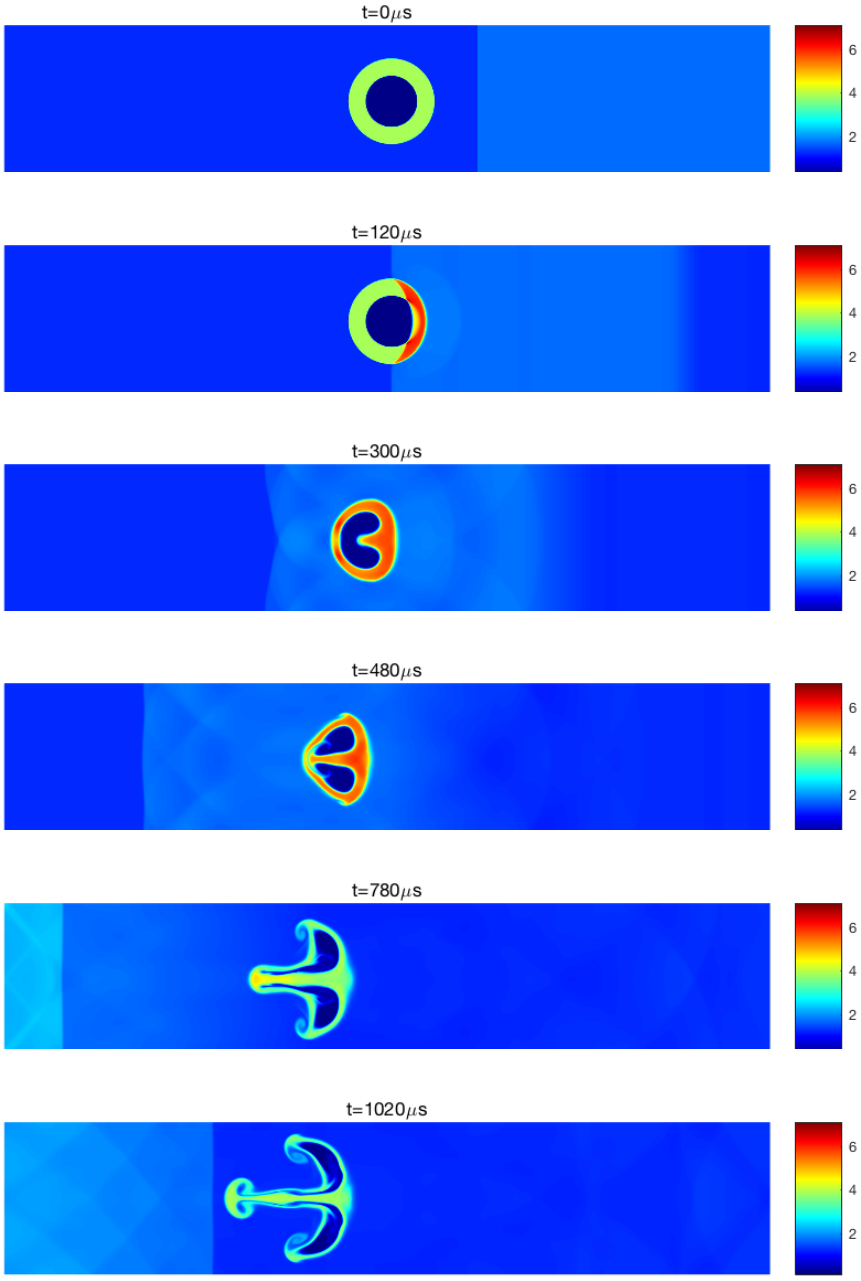

Figure 5: Results for a Mach 1.22 shock wave in air interacting with a Helium bubble with a R22 shell surrounding it (Experiment 5.1.3). Pseudo-color plots of the density at six different times $t = 0$, 120, 480, 780, and 1020 μs obtained with the numerical multiphase flow model with instantaneous pressure relaxation (1250×250 mesh).

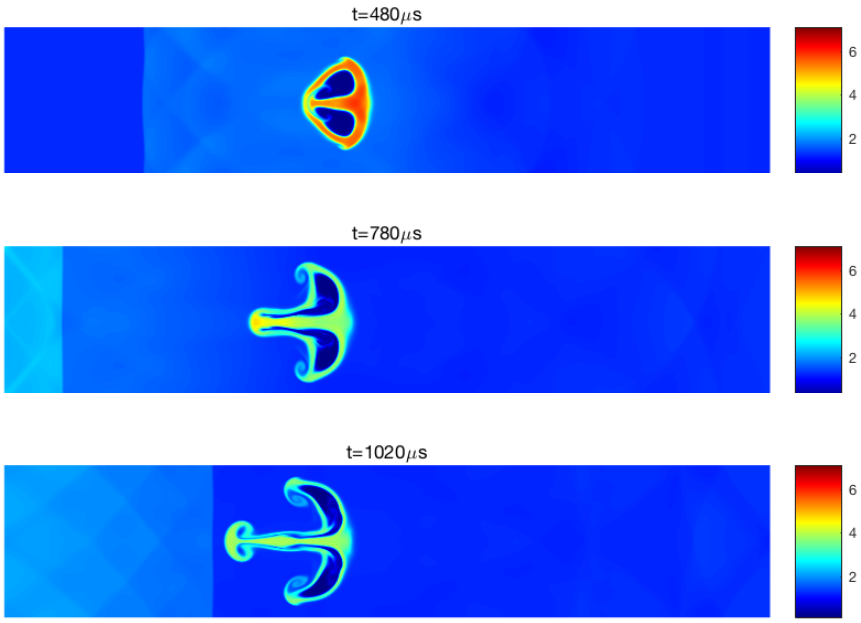

Figure 6: Results obtained using an extended transport five-equation model for the test problem considered in Fig. 5. Pseudo-color plots of the density are shown at three different times $t = 480$, 780, and 1020 μs (1250×250 mesh).

amount of air (non-condensable gas) with volume fraction $\alpha_g = 10^{-1}$. Air is modeled as an ideal gas, see Table 2 for the material-dependent parameters of the equations of state employed in this test. The initial pressure is $p_0 = 10^5$ Pa, and the initial densities correspond to the temperature $T_0 = 354$ K. A velocity discontinuity is set at initial time at the middle of the tube, with $u_0 = -20$ m/s on the left and $u_0 = 20$ m/s on the right. We use 3000 grid cells over the interval [0, 1] m, and Courant number = 0.5. We perform the simulation with different levels of activation of instantaneous relaxation processes:

(i) only mechanical relaxation (p-relaxation);
(ii) mechanical relaxation for all the three phases and thermal relaxation for the liquid-vapor pair only (pT(lv)-relaxation);
(iii) mechanical and thermal relaxation for all the phases (pT-relaxation);
(iv) mechanical relaxation for all the phases and thermal and chemical relaxation for the liquid-vapor pair (pT(lv)g-relaxation);
(v) mechanical and thermal relaxation for all the phases and chemical relaxation for the liquid-vapor pair (pTg-relaxation).

For the two cases (iv) and (v) of this cavitation tube test thermo-chemical relaxation is activated if the liquid temperature is greater than the saturation temperature at the local pressure, $T_{\text{liquid}} > T_{\text{sat}}(p)$. Second-order results are displayed at time $t = 6$ ms in Figure 7 for the pressure, the velocity, the total gaseous volume fraction $\alpha_{\text{wv}} + \alpha_g$, and the vapor mass fraction. In the same Figure 7 we also show the phasic temperatures for the two cases of p-relaxation and pTg-relaxation. In all the cases we observe two rarefactions propagating in opposite directions that

Table 2: Equation of state parameters employed in Section 5.2

k (phase)	γ	ϖ [Pa]	η [kJ/kg]	η' [kJ/(Kg · K)]	κ_v [J/(Kg · K)]
1 (vapor)	1.43	0	2030	−23.4	1040
2 (liquid)	2.35	10^9	−1167	0	1816
3 (gas)	1.4	0	0	0	718

produce a pressure decrease in the middle region of the tube, and, correspondingly, an increase of the total gaseous component. For the cases with activation of mass transfer, *i.e.*, pT(lv)g- and pTg-relaxation, two evaporation waves develop, causing an increase of the vapor mass fraction in the middle region. Note that in these cases the pressure decreases in the cavitation zone until the saturation value is reached, whereas the pressure reaches much lower values here if mass transfer is not activated. By inspecting the results we observe that the speed of the leading edges of the two rarefactions decreases for any additional instantaneous thermal equilibrium process that we activate in the computation, consistently with the sub-characteristic property demonstrated theoretically for the hierarchy of relaxed models in Section 3. Let us note that chemical relaxation is not active here around the rarefaction fronts since, as indicated above, mass transfer in this test is activated only in regions where $T_{\text{liquid}} > T_{\text{sat}}(p)$.

Experiment 5.2.2. We now perform a two-dimensional experiment. In this test we simulate a cylindrical underwater explosion (UNDEX) close to a rigid surface. Following [60], we consider an initial bubble of highly pressurized gas (combustion products) surrounded by liquid water and located near an upper flat wall. Three fluid components are involved in this problem: liquid water, water vapor, and combustion gases. We use a grid of 481×280 cells over the domain $[-0.6, 0.6] \times [-0.7, 0]\,\text{m}^2$. The bubble initially is located at $(x_\text{b}, y_\text{b}) = (0, -0.22)$ m, and it has radius $r_\text{b} = 0.05$ m. Inside the bubble we set initially a pressure $p = 8290 \times 10^5$ Pa, a gas density $\rho_\text{g} = 1400\,\text{kg/m}^3$, and volume fractions $\alpha_\text{wl} = \alpha_\text{wv} = 10^{-8}$ for the water phases. Outside the bubble we set $p = 10^5$ Pa, $T = 303$ K, and the volume fractions $\alpha_\text{wv} = 10^{-4}$ and $\alpha_\text{g} = 10^{-7}$, for water vapor and gas, respectively. The EOS parameters for water are those in Table 2. An ideal gas law is used for the combustion gases, with $\gamma_\text{g} = 2$. In this test we activate thermal and chemical relaxation for the liquid-vapor water pair. For comparison, we have also run a simulation with no thermo-chemical relaxation, this allowing us to highlight the effect of mass transfer processes. This explosion problem is characterized by a complex pattern of shocks and rarefaction waves [60], and the likely occurrence of creation and collapse of vapor cavities in the liquid region close to the wall, due to the strong rarefactions and subsequent recompression. We show in Figure 8 pseudo-color plots of the pressure at four different times obtained by activating thermo-chemical relaxation. At $t = 0.075$ ms (upper left plot) we can observe the circular shock created by the explosion. At $t = 0.2$ ms (upper right plot) this shock has reflected from the wall, at time $t = 0.35$ ms (lower left plot) a low pressure cavitation region has begun to develop close to the rigid surface, and this region is more extended at $t = 0.5$ ms (lower right plot). The thick solid circle line indicates the water/bubble interface. In Figure 9 we display the history in time of the pressure, the water vapor volume fraction and the water vapor mass fraction at the point $(0, 0)$ at the center of the wall. In these plots we also show the results of the computation done with no activation of mass transfer, in which case cavitation is a mechanical process only, and mass fractions do not vary. For the two computations, with and without mass transfer, we observe some common features: a pressure peak of the same magnitude corresponding to the instant at which the circular shock hits the wall, the drop of the pressure and consequent growth of a

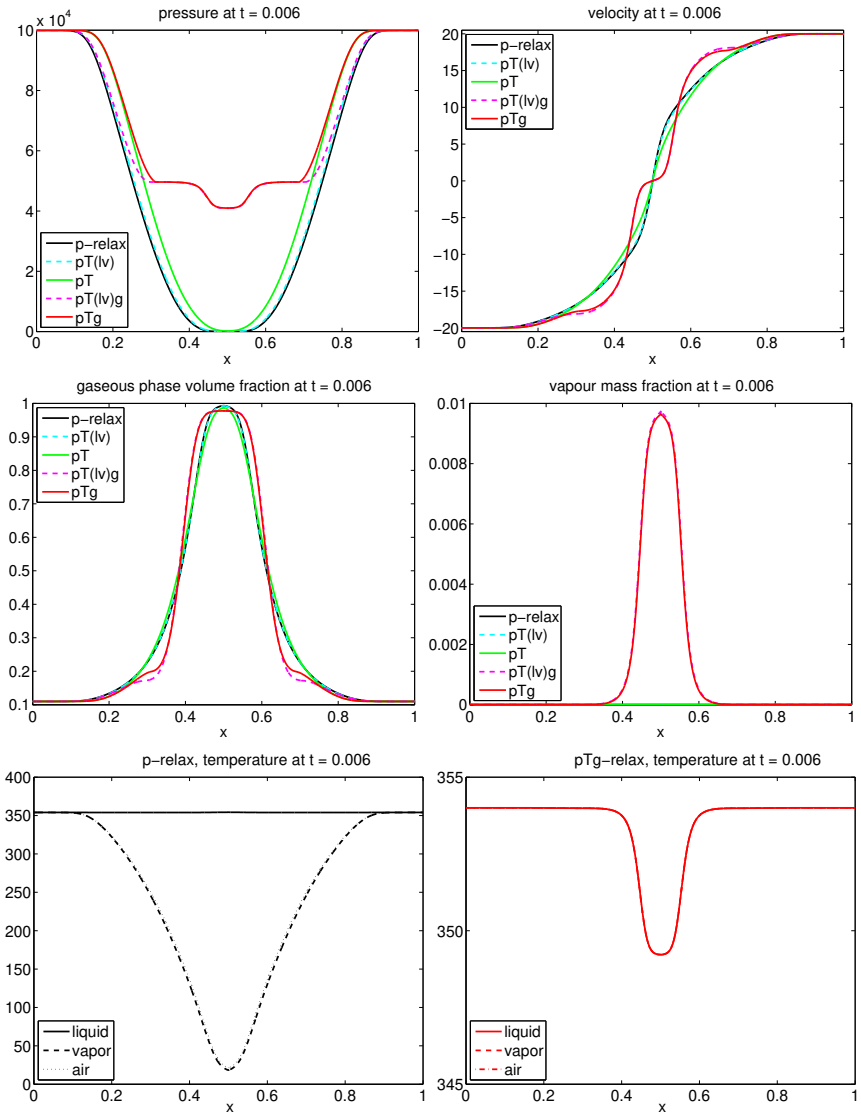

Figure 7: Numerical results for the three-phase cavitation tube test (Experiment 5.2.1). First and second row: results for the pressure, velocity, total gas volume fraction, and vapor mass fraction for the various relaxation cases. Third row: temperature of the three phases (liquid, vapor, air) for the p-relaxation case (left), and for the pTg-relaxation case (right).

gaseous region in this zone, which then disappears due to the subsequent recompression. Later, further weaker processes of cavitation formation and collapse are observed. The behavior of the vapor volume fraction is also qualitatively and quantitatively analogous in the two cases, with or without liquid-vapor transition. However, similar to what observed for the one-dimensional cavitation tube experiment (Experiment 5.2.1), the minimum pressure in the cavitation region has very different order of magnitude for the two computations, as we can observe from the zoom of the pressure history in time in Figure 9 (upper right plot). In fact, the pressure continues to decrease until very low values if no phase transition is activated, whereas it decreases until the saturation value otherwise. For instance, at the time $t = 0.529$ ms corresponding to the maximum value at the wall of the vapor volume fraction, we obtain a pressure $p = 28$ Pa with no mass transfer and $p = 4417$ Pa with mass transfer. In the literature these type of UNDEX problems are typically simulated by simpler single-fluid models [33, 60, 65, 58], or by two-phase flow models [13, 38, 21] that are only able to describe mechanical cavitation processes, that is growth/collapse of gas cavities due to pressure variations, with no liquid-vapor transition. In contrast, our three-phase flow model allows a more accurate description of the thermodynamics of cavitation processes, which involve liquid-vapor phase change. We notice that this is critical for an accurate prediction of the pressure field on the wall adjacent to cavitation regions. We have to remark however an important limit of our current numerical model in relation to the use of the simple stiffened gas EOS. This equation of state can be considered a linearized version of the Mie–Grüneisen EOS around a reference thermodynamic state [39]. While numerically convenient, this simple EOS is not suited for accurate predictions of flow conditions with significant variations of the thermodynamic variables, as we have in the UNDEX problems simulated here. The current numerical model with the SG EOS is nonetheless able to qualitatively describe the relevant physical phenomena and it allows us to better understand the effect of the activation of mass transfer processes.

Experiment 5.2.3. We finally simulate an underwater explosion problem similar to the previous one, but here we set a free surface instead of an upper rigid solid surface. Many authors in the literature have simulated numerically this type of problem, *e.g.* [34, 61, 62, 13, 21]. However, as for the previous test, simulations presented in the literature are typically based on simple single-fluid models or two-phase models that do not account for liquid-vapor transition. The setup of this problem has been chosen in order to be able to make qualitative comparisons with the laboratory underwater explosion test of Kleine *et al.* [25] (simulated also for instance in [13]). As before, we consider an initial bubble of highly pressurized gas surrounded by liquid water. Here the bubble is located near an air/water interface. Four fluid components are involved in this problem: liquid water, water vapor, combustion gases (the bubble), and air (region above the free surface). Since here we focus on phase transition phenomena triggered by the explosion, we make the simplifying assumption that the bubble consists of air at high pressure, so that we need to consider three phases only instead of four. Note that other authors choose to model the bubble by a high pressure liquid region [13]. We use a grid of 669×600 cells over the domain $[-0.09, 0.09]\times[-0.12, 0.042]\,\mathrm{m}^2$. The bubble initially is located at $(x_\mathrm{b}, y_\mathrm{b}) = (0, -0.034)$ m, and it has radius $r_\mathrm{b} = 0.0035$ m. The free surface is located at $y = 0$ m. Inside the bubble we set initially a pressure $p = 8290 \times 10^5$ Pa, a gas density $\rho_\mathrm{g} = 1400\,\mathrm{kg/m}^3$, and volume fractions $\alpha_\mathrm{wl} = 10^{-8}$ and $\alpha_\mathrm{wv} = 10^{-7}$ for the liquid and vapor phases of water. Outside the bubble, both below and above the free surface, we set $p = 10^5$ Pa and $T = 298$ K. In the air region above the free surface we set water volume fractions $\alpha_\mathrm{wl} = 10^{-8}$ (liquid) and $\alpha_\mathrm{wv} = 10^{-7}$ (vapor), while below the free surface we take $\alpha_\mathrm{wv} = 10^{-4}$ and $\alpha_\mathrm{g} = 10^{-7}$, for water vapor and air (inert gas), respectively. The EOS parameters for water are again those in Table 2. An ideal gas law is used for air

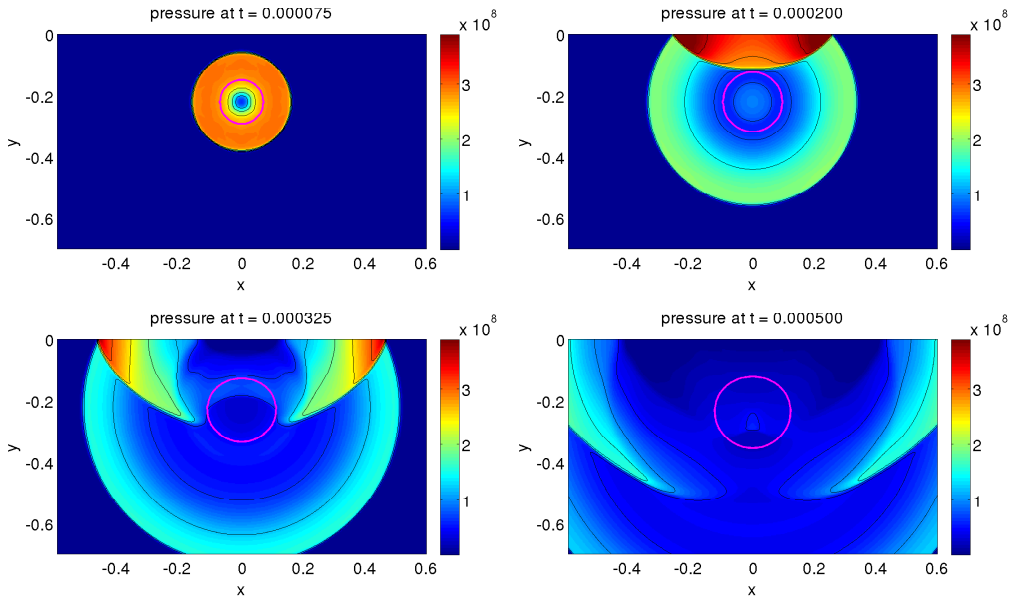

Figure 8: Numerical results for the UNDEX experiment near a rigid surface (Experiment 5.2.2). Pressure field at times t = 0.075, 0.2, 0.325, 0.5 ms computed by the HLLC-type scheme with activation of thermo-chemical relaxation for the liquid-vapor pair. The thick solid line (magenta color) indicates the water/bubble interface.

with $\gamma_g = 1.4$. Heat and mass transfer processes are activated in this test. The characteristic features of this explosive event near a free surface are similar to those of an event close to a wall: a circular blast wave is produced by the highly pressurized gas bubble, and it interacts with the air/water interface, leading to a reflected expansion wave. Due to the consequent pressure decrease, a cavitation region is formed just below the free surface. Our numerical model allows us to describe the liquid-vapor transition processes occurring in this region. We show in Figure 10 pseudo-color plots of the pressure and the vapor mass fraction at three different times, chosen to have snapshots comparable to the three frames of the Schlieren visualization of the experiment of Kleine *et al.* [25] (also reported in [13]). Moreover, in Figure 11 we also display the mixture density and the velocity field at final time. The latter plot in particular allows us to observe the transmitted shock wave in air, which is too weak to be seen in the plots of the pressure field. Despite the several simplifications in the model our simulation is able to reproduce qualitatively the main physical processes observed experimentally [25].

6. Conclusions

We have presented a numerical model for multiphase compressible flows involving the liquid and vapor phases of one species and one or more inert gaseous phases, extending the two-phase flow model that we have introduced in [45]. The model includes mechanical, thermal and chemical relaxation processes. We have also rigorously derived the associated pressure-relaxed model by asymptotic techniques, and carried an analysis of the characteristic speeds of the hierarchy of relaxed models associated to the parent model. The multiphase equations

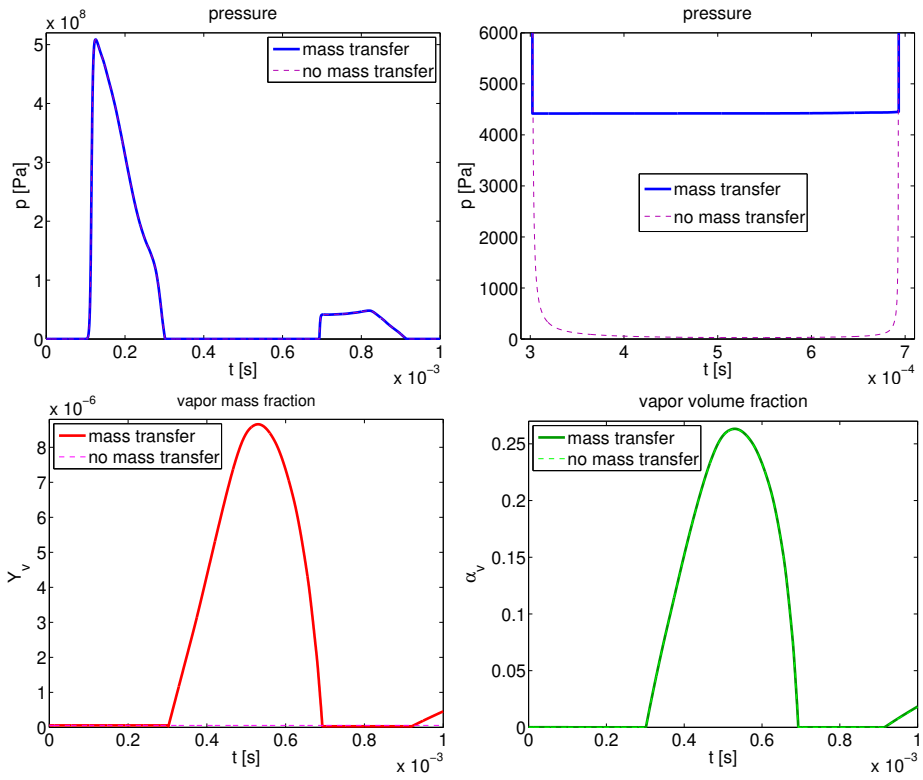

Figure 9: Numerical results for the UNDEX experiment near a rigid surface (Experiment 5.2.2). History in time at the point $(0, 0)$ at the center of the wall (solid line: with mass transfer, dashed line: no mass transfer). Top plots: Pressure, with a zoom in the cavitation region shown in the right plot. Bottom plots: vapor mass fraction (left) and vapor volume fraction (right).

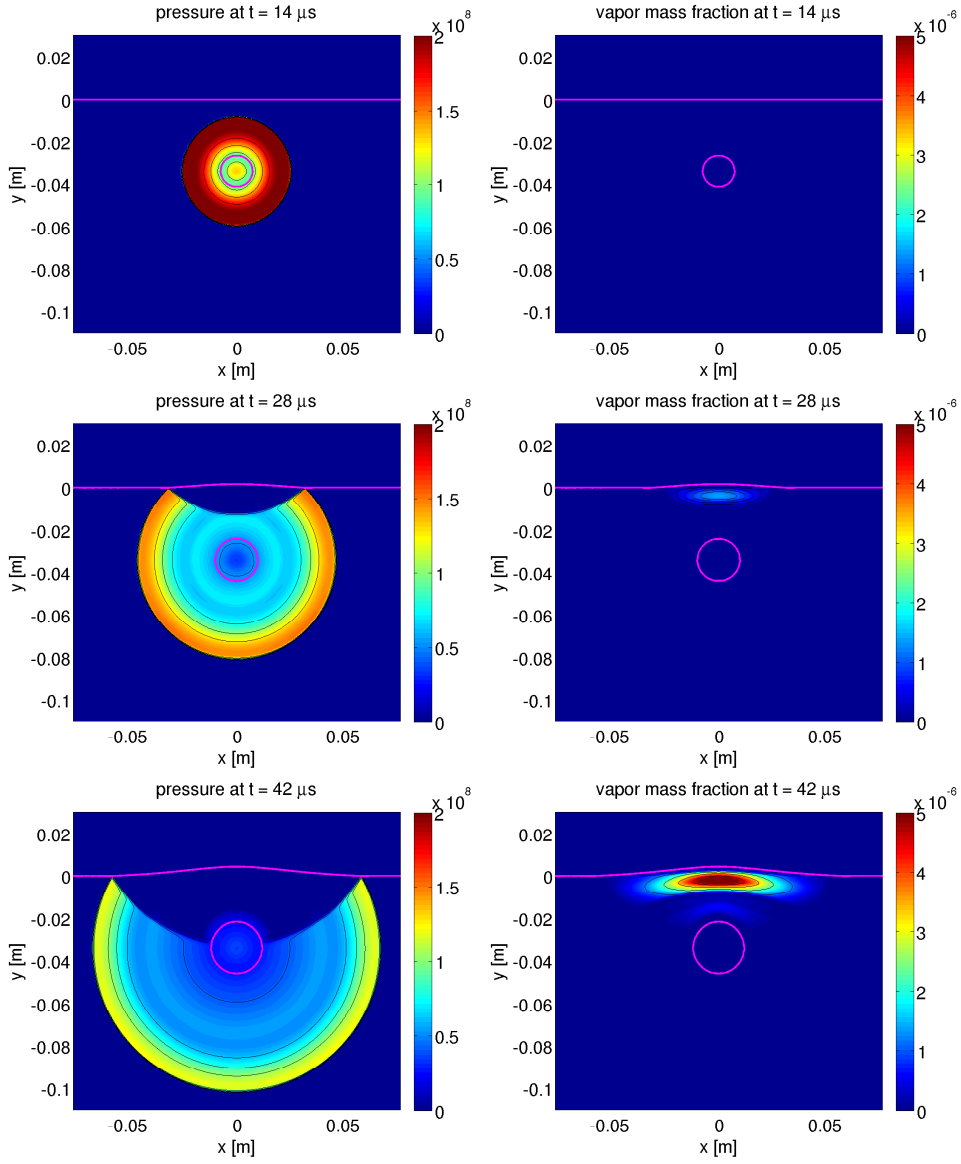

Figure 10: Numerical results for the UNDEX experiment near a free surface (Experiment 5.2.3). Pressure field (left column) and water vapor mass fraction (right column) at times $t = 14,\ 28,\ 42\,\mu s$ computed by the HLLC-type scheme with activation of thermo-chemical relaxation. The thick solid lines (magenta color) indicate the free surface and the water/bubble interface.

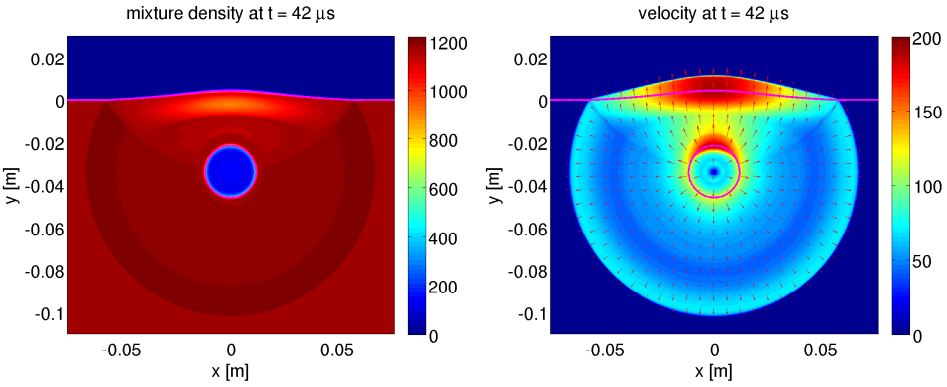

Figure 11: Numerical results for the UNDEX experiment near a free surface (Experiment 5.2.3). Results for the mixture density (left) and the velocity field (right) at $t = 42\,\mu s$. The thick solid lines (magenta color) indicate the free surface and the water/bubble interface.

are solved by a mixture-energy-consistent finite volume wave propagation scheme based on an original HLLC/Suliciu-type Riemann solver, combined with simple and robust procedures for the stiff relaxation terms. Sample one-dimensional tests show the agreement of the computed numerical solution with the exact solution for three-phase Riemann problems with mechanical and thermal equilibrium. A cavitation tube experiment also allows us to show that the behaviour of the wave speed predicted numerically is consistent with our theoretical findings on the sub-characteristic interlacing of the characteristic speeds for the hierarchy of relaxed models. The numerical results, finally, show the efficiency of the numerical method in modelling complex wave patterns, shocks and interfaces in problems with thermal and mass transfer processes where the dynamical appearance of vapor cavities and evaporation fronts in a liquid is coupled to the dynamics of a third non-condensable gaseous component governed by its own equation of state. An example of application illustrated in the present work is the simulation of underwater explosions close to a rigid wall or a free surface. In these problems a highly pressurized gas bubble triggers cavitation processes in a liquid. Another application example is the simulation of high speed cavitating underwater systems, considered for instance in [48]. Some limits of the numerical model presented in this work are the choice of a simple stiffened gas equation of state and the assumption of instantaneous heat and mass transfer. Future work will be dedicated to the extension of the model to more complex and general equations of state, such as the IAPWS Industrial Formulation for Water and Steam [57], and to finite-rate thermo-chemical relaxation processes.

Acknowledgments. The first author (M. Pelanti) was partially supported by the French Government Directorate for Armament (DGA) under Grant N. 2012.60.0011.00.470.75.01, and also partially supported by the Norwegian RCN Grant N. 234126/E30 in the framework of the SIMCOFLOW Project. The second author (K.-M. Shyue) was supported in part by the Ministry of Science and Technology of Taiwan under Grant N. 103-2115-M-002-011-MY2. M. Pelanti is grateful to Tore Flåtten and Gaute Linga for very fruitful discussions.

A. Derivation of the relaxed pressure-equilibrium model

In this section we derive the p-relaxed model in (11) from the multiphase model in (1). For simplicity, we shall consider the one-dimensional case $d = 1$. We follow in particular the technique of Murrone–Guillard [41] (see also [10]). First, we write the system (1) in one dimension in terms of the vector of primitive variables $w \in \mathbb{R}^{3N}$ as:

$$\partial_t w + A(w)\partial_x w = \frac{1}{\tau}\Psi(w) + \Phi(w), \tag{70a}$$

where $\tau \equiv 1/\mu$, and

$$w = \begin{bmatrix} \alpha_1 \\ \alpha_3 \\ \vdots \\ \alpha_N \\ \rho_1 \\ \rho_2 \\ \vdots \\ \rho_N \\ u \\ p_1 \\ p_2 \\ \vdots \\ p_N \end{bmatrix}, \quad A = \begin{bmatrix} u & 0 & \dots & 0 & 0 & 0 & \dots & 0 & 0 & 0 & 0 & \dots & 0 \\ 0 & u & \dots & 0 & 0 & 0 & \dots & 0 & 0 & 0 & 0 & \dots & 0 \\ \vdots & \vdots & \ddots & \vdots & \vdots & \vdots & \vdots & \vdots & \vdots & \vdots & \vdots & \vdots & \vdots \\ 0 & 0 & 0 & u & 0 & 0 & \dots & 0 & 0 & 0 & 0 & \dots & 0 \\ 0 & 0 & \dots & 0 & u & 0 & \dots & 0 & \rho_1 & 0 & 0 & \dots & 0 \\ 0 & 0 & \dots & 0 & 0 & u & \dots & 0 & \rho_2 & 0 & 0 & \dots & 0 \\ \vdots & \vdots & \vdots & \vdots & \vdots & \vdots & \ddots & \vdots & \vdots & \vdots & \vdots & \vdots & \vdots \\ 0 & 0 & \dots & 0 & 0 & 0 & \dots & u & \rho_N & 0 & 0 & \dots & 0 \\ \frac{p_1-p_2}{\rho} & \frac{p_3-p_2}{\rho} & \dots & \frac{p_N-p_2}{\rho} & 0 & 0 & \dots & 0 & u & \frac{\alpha_1}{\rho} & \frac{\alpha_2}{\rho} & \dots & \frac{\alpha_N}{\rho} \\ 0 & 0 & \dots & 0 & 0 & 0 & \dots & 0 & \rho_1 c_1^2 & 0 & 0 & \dots & 0 \\ 0 & 0 & \dots & 0 & 0 & 0 & \dots & 0 & \rho_2 c_2^2 & 0 & u & \dots & 0 \\ \vdots & \vdots & \vdots & \vdots & \vdots & \vdots & \vdots & \vdots & \vdots & \vdots & \vdots & \ddots & \vdots \\ 0 & 0 & \dots & 0 & 0 & 0 & \dots & 0 & \rho_N c_N^2 & 0 & 0 & \dots & u \end{bmatrix}, \tag{70b}$$

$$\Psi = \begin{bmatrix} \sum_{j=1}^N (p_1 - p_j) \\ \sum_{j=1}^N (p_3 - p_j) \\ \vdots \\ \sum_{j=1}^N (p_N - p_j) \\ -\frac{\rho_1}{\alpha_1} \sum_{j=1}^N (p_1 - p_j) \\ -\frac{\rho_2}{\alpha_2} \sum_{j=1}^N (p_2 - p_j) \\ \vdots \\ -\frac{\rho_N}{\alpha_N} \sum_{j=1}^N (p_N - p_j) \\ 0 \\ -\frac{1}{\alpha_1} \sum_{j=1}^N [\Gamma_1(\mathcal{E}_1 + p_{11j}) + \chi_1\rho_1](p_1 - p_j) \\ -\frac{1}{\alpha_2} \sum_{j=1}^N [\Gamma_2(\mathcal{E}_2 + p_{12j}) + \chi_2\rho_2](p_2 - p_j) \\ \vdots \\ -\frac{1}{\alpha_N} \sum_{j=1}^N [\Gamma_N(\mathcal{E}_N + p_{1Nj}) + \chi_N\rho_N](p_N - p_j) \end{bmatrix}, \quad \Phi = \begin{bmatrix} 0 \\ 0 \\ \vdots \\ 0 \\ \frac{\mathcal{M}}{\alpha_1} \\ -\frac{\mathcal{M}}{\alpha_2} \\ \vdots \\ 0 \\ 0 \\ \frac{\Gamma_1}{\alpha_1} \sum_{j=1}^N \mathcal{Q}_{1j} + (\Gamma_1 g_1 + \chi_1) \frac{\mathcal{M}}{\alpha_1} \\ \frac{\Gamma_2}{\alpha_2} \sum_{j=1}^N \mathcal{Q}_{2j} - (\Gamma_2 g_1 + \chi_2) \frac{\mathcal{M}}{\alpha_2} \\ \vdots \\ \frac{\Gamma_N}{\alpha_N} \sum_{j=1}^N \mathcal{Q}_{Nj} \end{bmatrix}. \tag{70c}$$

We are interested in the behavior of the solutions of (70) in the limit $\tau \to 0^+$ ($\mu = \frac{1}{\tau} \to +\infty$). We expect that these solutions are close to the set $\mathfrak{U} = \{w \in \mathbb{R}^{3N};\, \Psi(w) = 0\}$. We assume that the set of equations $\Psi(w) = 0$ defines a smooth manifold of dimension L and that for any $w \in \mathfrak{U}$ we know a parameterization Ξ (the Maxwellian) from an open subset Ω of $\mathbb{R}^L$ on a neighborhood of

w in $\mathfrak{U}$. For any $v \in \Omega \subset \mathbb{R}^L$ the Jacobian matrix $d\Xi_v$ is a full rank matrix, moreover, the column vectors of $d\Xi_v$ form a basis of $\ker(\Psi'(\Xi(v)))$ [41]. Now let us define the matrix $C \in \mathbb{R}^{3N\times 3N}$:

$$C = [d\Xi_v^1 \dots d\Xi_v^L \, V^1 \dots V^{3N-L}] \tag{71}$$

where $d\Xi_v^1, \dots, d\Xi_v^L$ are the column vectors of $d\Xi_v$ and $\{V^1, \dots, V^{3N-L}\}$ is a basis of the range of $\Psi'(\Xi(v))$. Based on the observations above, the matrix C is invertible. Let us now denote with P the $L \times 3N$ matrix composed of the first L rows of the inverse C^{-1}. We have also the following results (see [41]):

$$P\, d\Xi_v = \mathbb{I}_L \quad \text{and} \quad P\, \Psi'(\Xi(v)) = 0, \tag{72}$$

where $\mathbb{I}_L$ denotes the $L \times L$ identity matrix. Now to obtain a reduced pressure equilibrium model we look for solutions in the form $w = \Xi(v) + \tau z$, where z is a small perturbation around the equilibrium state $\Xi(v)$. Using this into the system (70) we obtain

$$\partial_t(\Xi(v)) + A(\Xi(v))\partial_x(\Xi(v)) - \Psi'(\Xi(v))\, z = \Phi(\Xi(v)) + O(\tau). \tag{73}$$

Multiplying the above equation by P, by using (72), and by neglecting terms of order τ, we obtain the reduced model system:

$$\partial_t v + PA(\Xi(v))d\Xi_v\partial_x v = P\Phi(\Xi(v)). \tag{74}$$

In the limit of instantaneous pressure relaxation we have $p_k = p, \forall k = 1, \dots, N$, hence the vector of the variables of the reduced pressure-relaxed model is

$$v = [\alpha_1, \alpha_3, \dots, \alpha_N, \rho_1, \rho_2, \dots, \rho_N, u, p]^{\mathrm{T}} \in \mathbb{R}^{2N+1}. \tag{75}$$

Note that here $L = 2N + 1$. The equilibrium state $\Xi(v)$ is defined by:

$$\Xi : v \to \Xi(v) = [\alpha_1, \alpha_3, \dots, \alpha_N, \rho_1, \rho_2, \dots, \rho_N, u, p, p, \dots, p]^{\mathrm{T}} \in \mathbb{R}^{3N}. \tag{76}$$

The Jacobian $d\Xi_v \in \mathbb{R}^{3N\times 2N+1}$ of the Maxwellian is:

$$d\Xi_v = \left[\begin{array}{ccc|c} & & & 0 \\ & \mathbb{I}_{2N} & & \vdots \\ & & & 0 \\ \hline 0 & \dots & 0 & 1 \\ & \ddots & & \vdots \\ 0 & \dots & 0 & 1 \end{array}\right]. \tag{77}$$

A basis $\{V^1, \dots, V^{N-1}\}$, $V^k \in \mathbb{R}^{3N}$, $k = 1, \dots, N-1$, for the range of $\Psi'(\Xi(v))$ is found as

$$V^1 = \begin{bmatrix} (N-1) \\ -1 \\ -1 \\ \vdots \\ -1 \\ -(N-1)\frac{\rho_1}{\alpha_1} \\ \frac{\rho_2}{\alpha_2} \\ \frac{\rho_3}{\alpha_3} \\ \vdots \\ \frac{\rho_N}{\alpha_N} \\ 0 \\ -(N-1)\frac{\rho_1}{\alpha_1}c_1^2 \\ \frac{\rho_2}{\alpha_2}c_2^2 \\ \frac{\rho_3}{\alpha_3}c_3^2 \\ \vdots \\ \frac{\rho_N}{\alpha_N}c_N^2 \end{bmatrix}, \quad V^2 = \begin{bmatrix} -1 \\ (N-1) \\ -1 \\ \vdots \\ -1 \\ \frac{\rho_1}{\alpha_1} \\ \frac{\rho_2}{\alpha_2} \\ -(N-1)\frac{\rho_3}{\alpha_3} \\ \vdots \\ \frac{\rho_N}{\alpha_N} \\ 0 \\ \frac{\rho_1}{\alpha_1}c_1^2 \\ \frac{\rho_2}{\alpha_2}c_2^2 \\ -(N-1)\frac{\rho_3}{\alpha_3}c_3^2 \\ \vdots \\ \frac{\rho_N}{\alpha_N}c_N^2 \end{bmatrix}, \quad \dots, V^{N-1} = \begin{bmatrix} -1 \\ -1 \\ -1 \\ \vdots \\ (N-1) \\ \frac{\rho_1}{\alpha_1} \\ \frac{\rho_2}{\alpha_2} \\ \frac{\rho_3}{\alpha_3} \\ \vdots \\ -(N-1)\frac{\rho_N}{\alpha_N} \\ 0 \\ \frac{\rho_1}{\alpha_1}c_1^2 \\ \frac{\rho_2}{\alpha_2}c_2^2 \\ \frac{\rho_3}{\alpha_3}c_3^2 \\ \vdots \\ -(N-1)\frac{\rho_N}{\alpha_N}c_N^2 \end{bmatrix}. \tag{78}$$

Note that this structure is associated to the choice of the independent variables in w (where in particular we have chosen α_k, $k \neq 2$). Hence we can construct the matrix $C \in \mathbb{R}^{3N\times 3N}$ (71), compute the inverse C^{-1}, and finally obtain the matrix $P \in \mathbb{R}^{2N+1\times 3N}$ by taking the first $2N+1$ rows of C^{-1}. We find:

$$P = \left[\begin{array}{c|ccccc} & \frac{\alpha_1}{\rho_1 c_1^2}\rho c_p^2 \sum_{j=2}^N \frac{\alpha_j}{\rho_j c_j^2} & -\frac{\alpha_1\alpha_2}{\rho_1 c_1^2 \rho_2 c_2^2}\rho c_p^2 & -\frac{\alpha_1\alpha_3}{\rho_1 c_1^2 \rho_3 c_3^2}\rho c_p^2 & \dots & -\frac{\alpha_1\alpha_N}{\rho_1 c_1^2 \rho_N c_N^2}\rho c_p^2 \\ & -\frac{\alpha_1\alpha_3}{\rho_1 c_1^2 \rho_3 c_3^2}\rho c_p^2 & -\frac{\alpha_2\alpha_3}{\rho_2 c_2^2 \rho_3 c_3^2}\rho c_p^2 & \frac{\alpha_3}{\rho_3 c_3^2}\rho c_p^2 \sum_{\substack{j=1 \\ j\neq 3}}^N \frac{\alpha_j}{\rho_j c_j^2} & \dots & -\frac{\alpha_3\alpha_N}{\rho_3 c_3^2 \rho_N c_N^2}\rho c_p^2 \\ & \vdots & \vdots & \vdots & \vdots & \vdots \\ & -\frac{\alpha_1\alpha_N}{\rho_1 c_1^2 \rho_N c_N^2}\rho c_p^2 & -\frac{\alpha_2\alpha_N}{\rho_2 c_2^2 \rho_N c_N^2}\rho c_p^2 & -\frac{\alpha_3\alpha_N}{\rho_3 c_3^2 \rho_N c_N^2}\rho c_p^2 & \dots & \frac{\alpha_N}{\rho_N c_N^2}\rho c_p^2 \sum_{j=1}^{N-1} \frac{\alpha_j}{\rho_j c_j^2} \\ \mathbb{I}_{2N} & -\frac{1}{c_1^2}\rho c_p^2 \sum_{j=2}^N \frac{\alpha_j}{\rho_j c_j^2} & \frac{\alpha_2}{c_1^2 \rho_2 c_2^2}\rho c_p^2 & \frac{\alpha_3}{c_1^2 \rho_3 c_3^2}\rho c_p^2 & \dots & \frac{\alpha_N}{c_1^2 \rho_N c_N^2}\rho c_p^2 \\ & \frac{\alpha_1}{\rho_1 c_1^2 c_2^2}\rho c_p^2 & -\frac{1}{c_2^2}\rho c_p^2 \sum_{\substack{j=1 \\ j\neq 2}}^N \frac{\alpha_j}{\rho_j c_j^2} & \frac{\alpha_3}{c_2^2 \rho_3 c_3^2}\rho c_p^2 & \dots & \frac{\alpha_N}{c_2^2 \rho_N c_N^2}\rho c_p^2 \\ & \vdots & \vdots & \vdots & \vdots & \vdots \\ & \frac{\alpha_1}{\rho_1 c_1^2 c_N^2}\rho c_p^2 & \frac{\alpha_2}{\rho_2 c_2^2 c_N^2}\rho c_p^2 & \frac{\alpha_3}{\rho_3 c_3^2 c_N^2}\rho c_p^2 & \dots & -\frac{1}{c_N^2}\rho c_p^2 \sum_{j=1}^{N-1} \frac{\alpha_j}{\rho_j c_j^2} \\ & 0 & 0 & 0 & \dots & 0 \\ \hline 0\dots 0 & \rho c_p^2 \frac{\alpha_1}{\rho_1 c_1^2} & \rho c_p^2 \frac{\alpha_2}{\rho_2 c_2^2} & \rho c_p^2 \frac{\alpha_3}{\rho_3 c_3^2} & \dots & \rho c_p^2 \frac{\alpha_N}{\rho_N c_N^2} \end{array}\right], \tag{79}$$

where c_p is the speed of sound of the pressure-equilibrium model in (14). Finally, the reduced p-relaxed multiphase flow model in (11) is obtained from (74) by using the above expression of the matrix P and by evaluating the matrix A and the source term Φ in the equilibrium state $\Xi(v)$ in (76). Let us also note that we use the relations $\chi_k = c_k^2 - \Gamma_k h_k$ in the entries of Φ in (70c).

B. Speed of sound for the hierarchy of multiphase flow models

In this section we show the derivation of the expressions of the sound speed in (14), (19), and (26), following in particular the work in [19]. For the two-phase case, these formulas have been derived by various authors, see especially [59, 53, 18]. For flow models with $N \geq 2$ phases, the expression of the speed of sound have been studied in [19] for the case of instantaneous mechanical equilibrium and the case of both mechanical and thermal equilibrium for all the phases. The novelty here is the derivation of (26) for the flow model with chemical potential equilibrium and the generalization of (19) to the situation where only $2 \leq M < N$ phase are in thermal equilibrium. We begin by recalling some definitions and by writing some useful equalities:

$$c_k^2 = \left(\frac{\partial p_k}{\partial \rho_k}\right)_{s_k}, \quad \Gamma_k = \left(\frac{\partial p_k}{\partial \mathcal{E}_k}\right)_{\rho_k} = \frac{\rho_k}{T_k}\left(\frac{\partial T_k}{\partial \rho_k}\right)_{s_k}, \quad \kappa_{pk} = \left(\frac{\partial h_k}{\partial T_k}\right)_{p_k} = T_k\left(\frac{\partial s_k}{\partial T_k}\right)_{p_k}, \tag{80a}$$

$$\left(\frac{\partial T_k}{\partial p_k}\right)_{s_k} = \frac{T_k\Gamma_k}{\rho_k c_k^2}, \quad \left(\frac{\partial \rho_k}{\partial s_k}\right)_{p_k} = -\frac{T_k\Gamma_k\rho_k}{c_k^2}. \tag{80b}$$

Here a common pressure will be always assumed, $p_k = p$, $\forall k = 1, \ldots, N$. Now, by recalling $\rho = \sum_{k=1}^N \alpha_k\rho_k$ and $\sum_{k=1}^N \alpha_k = 1$, we can write:

$$\sum_{k=1}^N \frac{d(\alpha_k\rho_k)}{\rho_k} = \sum_{k=1}^N \frac{\alpha_k}{\rho_k} d\rho_k = \rho \sum_{k=1}^N \frac{1}{\rho_k} dY_k + \frac{1}{\rho} d\rho\,. \tag{81}$$

Hence:

$$\frac{1}{\rho} d\rho = \sum_{k=1}^N \frac{\alpha_k}{\rho_k} d\rho_k - \rho \sum_{k=1}^N \frac{1}{\rho_k} dY_k\,. \tag{82}$$

Then we can write, by considering $\rho_k = \rho_k(p, s_k)$:

$$d\rho_k = \left(\frac{\partial \rho_k}{\partial p}\right)_{s_k} dp + \left(\frac{\partial \rho_k}{\partial s_k}\right)_p ds_k = \frac{1}{c_k^2} dp - \frac{T_k\Gamma_k\rho_k}{c_k^2} ds_k\,. \tag{83}$$

Hence we obtain:

$$d\rho = \rho\left[\left(\sum_{k=1}^N \frac{\alpha_k}{\rho_k c_k^2}\right) dp - \sum_{k=1}^N \alpha_k \frac{T_k\Gamma_k}{c_k^2} ds_k - \rho \sum_{k=1}^N \frac{1}{\rho_k} dY_k\right]. \tag{84}$$

B.1. p-relaxation

Let us consider the pressure equilibrium model (11) (p-relaxed model). The speed of sound is defined in (13). Since in this definition we consider $ds_k = 0$ and $dY_k = 0$, $k = 1, \ldots, N$, from (84) we obtain the expression of the speed of sound c_p in (14).

B.2. pT-relaxation

We now consider pressure equilibrium for all the N phases, and, in addition, we assume that M phases, $2 \leq M \leq N$, are in thermal equilibrium at a common temperature T, $T_k = T$ for

$k = 1, \ldots, M$. Recalling the expression of the mixture specific total entropy $s = \sum_{k=1}^{N} Y_k s_k$, we can write

$$\sum_{k=1}^{M} Y_k ds_k = ds - \sum_{k=1}^{N} s_k dY_k - \sum_{k=M+1}^{N} Y_k ds_k \,. \tag{85}$$

By considering $T = T(p, s_k)$, then we can write

$$dT = \left(\frac{\partial T}{\partial p}\right)_{s_k} dp + \left(\frac{\partial T}{\partial s_k}\right)_{p} ds_k = \frac{T\Gamma_k}{\rho_k c_k^2} dp + \frac{T}{\kappa_{pk}} ds_k, \quad k = 1, \ldots, M. \tag{86}$$

Hence we obtain $M - 1$ equations:

$$\frac{1}{\kappa_{pk}} ds_k - \frac{1}{\kappa_{pk+1}} ds_{k+1} = \left(\frac{\Gamma_{k+1}}{\rho_{k+1} c_{k+1}^2} - \frac{\Gamma_k}{\rho_k c_k^2}\right), \quad k = 1, \ldots, M-1. \tag{87}$$

These $M - 1$ equations together with the equation (85) form a system of M equations for the unknowns $ds_k, k = 1, \ldots, M$ (the phasic entropy differentials for the M phases in both mechanical and thermal equilibrium). The solution of this system gives, after some manipulations:

$$ds_k = \frac{1}{\alpha_k \rho_k \sum_{j=1}^{M} C_{pj}} \left[C_{pk} \rho \left(ds - \sum_{j=1}^{N} s_j dY_j - \sum_{j=M+1}^{N} Y_j ds_j \right) + C_{pk} \sum_{j=1}^{M} \left(\frac{\Gamma_j}{\rho_j c_j^2} - \frac{\Gamma_k}{\rho_k c_k^2} \right) C_{pj} dp \right], \tag{88}$$

for $k = 1, \ldots, M$. Here we recall that $C_{pk} = \alpha_k \rho_k \kappa_{pk}$ (heat capacities). By introducing (88) in (84) we then obtain

$$\begin{aligned} d\rho = \rho \Bigg\{ & \left(\sum_{k=1}^{N} \frac{\alpha_k}{\rho_k c_k^2} \right) dp + T \frac{1}{\sum_{k=1}^{M} C_{pk}} \left[\sum_{k=1}^{M-1} C_{pk} \sum_{j=k+1}^{M} C_{pj} \left(\frac{\Gamma_j}{\rho_j c_j^2} - \frac{\Gamma_k}{\rho_k c_k^2} \right)^2 dp \right. \\ & \left. - \rho \sum_{k=1}^{M} \frac{\Gamma_k}{\rho_k c_k^2} C_{pk} \left(ds - \sum_{k=1}^{N} s_k dY_k - \sum_{k=M+1}^{N} Y_k ds_k \right) \right] - \sum_{k=M+1}^{N} \alpha_k \frac{T_k \Gamma_k}{c_k^2} ds_k - \rho \sum_{k=1}^{N} \frac{1}{\rho_k} dY_k \Bigg\}. \end{aligned} \tag{89}$$

The speed of sound $C_{pT,M}$ of the model with pressure equilibrium for all the phases and temperature equilibrium for $M \leq N$ phases is defined in (18). Since in this definition we consider $ds = 0$, $ds_k = 0$ for $k = M + 1, \ldots, N$, and $dY_k = 0$, for $k = 1, \ldots, N$, from (89) we obtain the expression of the speed of sound $c_{pT,M}$ in (19), by using also (14).

B.3. pTg-relaxation

We now consider pressure equilibrium for all the N phases, thermal equilibrium at temperature T for $M \leq N$ phases, $T_k = T$, for $k = 1, \ldots, M$, and chemical potential equilibrium for the liquid and vapor phase pair $(1, 2)$, $g_1 = g_2$ (note that this pair is also considered in thermal equilibrium). The speed of sound is defined in (25). Since in this definition we consider $ds = 0$, $ds_k = 0$ for $k = M + 1, \ldots, N$, and $dY_k = 0$, for $k = 3, \ldots, N$, we can write from (89):

$$\begin{aligned} d\rho = \rho \Bigg\{ & \left(\sum_{k=1}^{N} \frac{\alpha_k}{\rho_k c_k^2} \right) dp + T \frac{1}{\sum_{k=1}^{M} C_{pk}} \left[\sum_{k=1}^{M-1} C_{pk} \sum_{j=k+1}^{M} C_{pj} \left(\frac{\Gamma_j}{\rho_j c_j^2} - \frac{\Gamma_k}{\rho_k c_k^2} \right)^2 dp \right. \\ & \left. - \rho \sum_{k=1}^{M} \frac{\Gamma_k}{\rho_k c_k^2} C_{pk} (s_2 - s_1) dY_1 \right] - \rho \left(\frac{1}{\rho_1} - \frac{1}{\rho_2} \right) dY_1 \Bigg\}, \end{aligned} \tag{90}$$

where we have used $dY_2 = -dY_1$. Now we use the condition $d(g_1 - g_2) = 0$ to find a suitable expression for dY_1 in (90) as a function of dp. By recalling that $g_k = \varepsilon_k + \frac{p}{\rho_k} - T s_k$ and by noticing that $dg_k = \frac{1}{\rho_k} dp - s_k dT$, $k = 1, 2$, we can write:

$$d(g_2 - g_1) = \left(\frac{1}{\rho_2} - \frac{1}{\rho_1} \right) dp - (s_2 - s_1) dT. \tag{91}$$

We observe that dT can be expressed as:

$$dT = \frac{T\Gamma_1}{\rho_1 c_1^2} dp + \frac{T}{\kappa_{p1}} ds_1 \,. \tag{92}$$

By using here the expression for ds_1 given in (88) (with $ds = 0$, $ds_k = 0$ for $k = M+1, \ldots, N$, $dY_k = 0$, for $k = 3, \ldots, N$, $dY_1 = -dY_2$), we then obtain:

$$dT = \frac{\rho T}{\sum_{k=1}^{M} C_{pk}} \left[(s_2 - s_1) dY_1 + \frac{1}{\rho} \sum_{k=1}^{M} \frac{C_{pk}\Gamma_k}{\rho_k c_k^2} dp \right]. \tag{93}$$

Now we use this expression for dT in (91) and we solve $d(g_2 - g_1) = 0$ for the unknown dY_1, obtaining:

$$dY_1 = \frac{1}{\rho} \left[\left(\frac{1}{\rho_2} - \frac{1}{\rho_1} \right) \frac{1}{T(s_2 - s_1)^2} \sum_{k=1}^{M} C_{pk} - \frac{1}{s_2 - s_1} \sum_{k=1}^{M} \frac{C_{pk}\Gamma_k}{\rho_k c_k^2} \right] dp. \tag{94}$$

By introducing this equation in (90) and after some manipulations we obtain:

$$\begin{aligned} d\rho = \rho \Bigg\{ & \left(\sum_{k=1}^{N} \frac{\alpha_k}{\rho_k c_k^2} \right) dp + T \frac{1}{\sum_{k=1}^{M} C_{pk}} \left[\sum_{k=1}^{M-1} C_{pk} \sum_{j=k+1}^{M} C_{pj} \left(\frac{\Gamma_j}{\rho_j c_j^2} - \frac{\Gamma_k}{\rho_k c_k^2} \right)^2 dp \right. \\ & \left. + \left(\sum_{k=1}^{M} \frac{\Gamma_k C_{pk}}{\rho_k c_k^2} - \left(\frac{1}{\rho_2} - \frac{1}{\rho_1} \right) \frac{1}{T(s_2 - s_1)} \sum_{k=1}^{M} C_{pk} \right)^2 dp \right] \Bigg\}. \end{aligned} \tag{95}$$

With this result, we finally obtain the expression of the speed of sound $c_{pTg,M}$ in (26) by using the Clausius–Clapeyron equation

$$\left(\frac{dp}{dT} \right)_{\text{sat}} = (s_2 - s_1) \left(\frac{1}{\rho_2} - \frac{1}{\rho_1} \right)^{-1}. \tag{96}$$

References

[1] R. Abgrall and S. Karni. A comment on the computation of non-conservative products. *J. Comput. Phys.*, 229(8):2759–2763, 2010.

[2] R. Abgrall and H. Kumar. Numerical approximation of a compressible multiphase system. *Commun. Comput. Phys.*, 15(5):1237–1265, 2014.

[3] G. Allaire, S. Clerc, and S. Kokh. A five-equation model for the simulation of interfaces between compressible fluids. *J. Comput. Phys.*, 181:577–616, 2002.

[4] M. R. Baer and J. W. Nunziato. A two-phase mixture theory for the deflagration-to-detonation transition (DDT) in reactive granular materials. *Intl. J. Multiphase Flows*, 12:861–889, 1986.

[5] P. Batten, N. Clarke, C. Lambert, and D.M. Causon. On the choice of wavespeeds for the HLLC Riemann solver. *SIAM J. Sci. Comput.*, 18(6):1553–1570, 1997.
[6] M. Battistoni, D. Duke, A. B. Swantek, F. Zak Tilocco, C. F. Powell, and S. Som. Effects on noncondensable gas on cavitating nozzles. *Atomization Spray*, 25(6):453–483, 2015.
[7] M. Billaud Friess and S. Kokh. Simulation of sharp interface multi-material flows involving an arbitrary number of components through an extended five-equation model. *J. Comput. Phys.*, 273:488–519, 2014.
[8] F. Bouchut. *Nonlinear stability of finite volume methods for hyperbolic conservation laws, and well-balanced schemes for sources*. Birkhäuser-Verlag, 2004.
[9] M. J. Castro, P. LeFloch, M. L. Muñoz-Ruiz, and C. Parés. Why many theories of shock waves are necessary: Convergence error in formally path-consistent schemes. *J. Comput. Phys.*, 227:8107–8129, 2008.
[10] G. Q. Chen, C. D. Levermore, and T. P. Liu. Hyperbolic conservation laws with stiff relaxation terms and entropy. *Comm. Pure Appl. Math.*, 47:787–830, 1994.
[11] R. H. Cole. *Underwater Explosions*. Princeton University Press, 1948.
[12] G. Dal Maso, P. G. LeFloch, and F. Murat. Definition and weak stability of nonconservative products. *J. Math. Pures Appl.*, 74:483–548, 1995.
[13] A. Daramizadeh and M.R. Ansari. Numerical simulation of underwater explosion near air-water free surface using a five-equation reduced model. *Ocean Eng.*, 110:25–35, 2015.
[14] S. F. Davis. Simplified second-order Godunov-type methods. *SIAM J. Sci. Stat. Comput.*, 9:445–473, 1988.
[15] M. De Lorenzo, M. Pelanti, and P. Lafon. HLLC-type and path-conservative schemes for a single-velocity six-equation two-phase flow model: A comparative study. *Appl. Math. Comp.*, 333:95–117, 2018.
[16] M. Dumbser and D. S. Balsara. A new efficient formulation of the HLLEM Riemann solver for general conservative and non-conservative hyperbolic systems. *J. Comput. Phys.*, 304:275–319, 2016.
[17] M. Dumbser and E. F. Toro. A simple extension of the Osher Riemann solver to non-conservative hyperbolic systems. *J. Sci. Comput.*, 48:70–88, 2011.
[18] T. Flåtten and H. Lund. Relaxation two-phase models and the subcharacteristic condition. *Math. Models Methods Appl. Sci.*, 21:2379–2407, 2011.
[19] T. Flåtten, A. Morin, and S.T. Munkejord. Wave propagation in multicomponent flow models. *SIAM J. Appl. Math.*, 8:2861–2882, 2010.
[20] E. Godlewski and P.-A. Raviart. *Numerical Approximation of Hyperbolic Systems of Conservation Laws*. Springer-Verlag, New York, 1996.
[21] O. Haimovich and H. Frankel. Numerical simulations of compressible multicomponent and multiphase flow using a high-order targeted ENO (TENO) finite-volume method. *Computers and Fluids*, 146:105–116, 2017.
[22] S. Jin and Z. P. Xin. The relaxation schemes for systems of conservation laws in arbitrary space dimensions. *Comm. Pure Appl. Math.*, 48:235–276, 1995.
[23] A.K. Kapila, R. Menikoff, J. B. Bdzil, S. F. Son, and D.S. Stewart. Two-phase modeling of deflagration-to-detonation transition in granular materials: Reduced equations. *Physics of Fluids*, 13:3002–3024, 2001.
[24] V. K. Kedrinskiy. *Hydrodynamics of Explosion. Experiments and models*. Springer, 2005.
[25] H. Kleine, S. Tepper, K. Takehara, T. G. Etoh, and K. Hiraki. Cavitation induced by low speed underwater impact. In *Shock Waves: 26th International Symposium on Shock Waves, Vol. 2*, pages 895–900. Springer, 2009.
[26] O. Le Métayer, J. Massoni, and R. Saurel. Elaborating equations of state of a liquid and its vapor for two-phase flow models. *Int. J. Therm. Sci.*, 43:265–276, 2004.
[27] O. Le Métayer, J. Massoni, and R. Saurel. Dynamic relaxation processes in compressible multiphase flows. application to evaporation phenomena. *ESAIM: Proc.*, 40:103–123, 2013.
[28] R. J. LeVeque. CLAWPACK. `http://www.clawpack.org`.
[29] R. J. LeVeque. Wave propagation algorithms for multi-dimensional hyperbolic systems. *J. Comput. Phys.*, 131:327–353, 1997.
[30] R. J. LeVeque. *Finite Volume Methods for Hyperbolic Problems*. Cambridge University Press, 2002.
[31] R. J. LeVeque and M. Pelanti. A class of approximate Riemann solvers and their relation to relaxation schemes. *J. Comput. Phys.*, 172:572–591, 2001.
[32] G. Linga. A hierarchy of non-equilibrium two-phase flow models, 2018. preprint.
[33] T. G. Liu, B. C. Khoo, and W. F. Xie. Isentropic one-fluid modelling of unsteady cavitating flow. *J. Comput. Phys.*, 201:80–108, 2004.
[34] T. G. Liu, B. C. Khoo, and K. S. Yeo. The simulation of compressible multi-medium flow, II: Applications to 2D underwater shock refraction. *Computers and Fluids*, 57:291–314, 2001.
[35] T. P. Liu. Hyperbolic conservation laws with relaxation. *Comm. Math. Phys.*, 108:153–175, 1987.
[36] H. Lund. A hierarchy of relaxation models for two-phase flows. *SIAM J. Appl. Math.*, 72(6):1713–1741, 2012.
[37] H. Lund and P. Aursand. Two-phase flow of CO_2 with phase transfer. *Energy Procedia*, 23:246–255, 2012.
[38] Z. H. Ma, D. M. Causon, L. Qian, H. B. Gu, C. G. Mingham, and P. Martínez Ferrer. A GPU based compressible multiphase hydrocode for modelling violent hydrodynamic impact problems. *Computers and Fluids*, 120:1–23,

2015.
[39] R. Menikoff and B. J. Plohr. The Riemann problem for fluid flow of real materials. *Rev. Modern Phys.*, 61:75–130, 1989.
[40] A. Morin, P. K. Aursand, T. Flåtten, and S. T. Munkejord. Numerical resolution of CO_2 transport dynamics. In *SIAM Conference on Mathematics for Industry: Challenges and Frontiers (MI09), San Francisco, CA, USA*, 2009.
[41] A. Murrone and H. Guillard. A five equation reduced model for compressible two phase flow problems. *J. Comput. Phys.*, 202:664–698, 2005.
[42] C. Parés. Numerical methods for nonconservative hyperbolic systems: a theoretical framework. *SIAM J. Numer. Anal.*, 44:300–321, 2006.
[43] M. Pelanti. Low Mach number preconditioning techniques for Roe-type and HLLC-type methods for a two-phase compressible flow model. *Appl. Math. Comp.*, 310:112–133, 2017.
[44] M. Pelanti and K.-M. Shyue. A mixture-energy-consistent numerical approximation of a two-phase flow model for fluids with interfaces and cavitation. In *Hyperbolic Problems: Theory, Numerics, Applications, Proc. 14th Intl. Conf. on Hyperbolic Problems*, pages 839–846. AIMS, 2014.
[45] M. Pelanti and K.-M. Shyue. A mixture-energy-consistent six-equation two-phase numerical model for fluids with interfaces, cavitation and evaporation waves. *J. Comput. Phys.*, 259:331–357, 2014.
[46] O. E. Petel and F. X. Jetté. Comparison of methods for calculating the shock Hugoniot of mixtures. *Shock Waves*, 20:73–83, 2010.
[47] F. Petitpas, E. Franquet, R. Saurel, and O. Le Métayer. A relaxation-projection method for compressible flows. Part II: Artificial heat exchanges for multiphase shocks. *J. Comput. Phys.*, 225(2):2214–2248, 2007.
[48] F. Petitpas, J. Massoni, R. Saurel, E. Lapebie, and L. Munier. Diffuse interface models for high speed cavitating underwater systems. *Int. Journal Multiphase Flows*, 35(8):747–759, 2009.
[49] R. Saurel, P. Boivin, and O. LeMétayer. A general formulation for cavitating, boiling and evaporating flows. *Computers and Fluids*, 128:53–64, 2016.
[50] R. Saurel, O. Le Métayer, J. Massoni, and S. Gavrilyuk. Shock jump relations for multiphase mixtures with stiff mechanical relaxation. *Shock Waves*, 16:209–232, 2007.
[51] R. Saurel, F. Petitpas, and R. Abgrall. Modelling phase transition in metastable liquids: application to cavitating and flashing flows. *J. Fluid Mech.*, 607:313–350, 2008.
[52] R. Saurel, F. Petitpas, and R. A. Berry. Simple and efficient relaxation methods for interfaces separating compressible fluids, cavitating flows and shocks in multiphase mixture. *J. Comput. Phys.*, 228:1678–1712, 2009.
[53] H. B. Stewart and B. Wendroff. Two-phase flow: models and methods. *J. Comput. Phys.*, 56:363–409, 1984.
[54] S. A. Tokareva and E. F. Toro. HLLC-type Riemann solver for the Baer-Nunziato equations of compressible two-phase flow. *J. Comput. Phys.*, 229:3573–3604, 2010.
[55] E. F. Toro. *Riemann Solvers and Numerical Methods for Fluid Dynamics*. Springer-Verlag, Berlin, Heidelberg, 1997.
[56] E. F. Toro, M. Spruce, and W. Speares. Restoration of the contact surface in the HLL Riemann solver. *Shock Waves*, 4:25–34, 1994.
[57] W. Wagner, J. R. Cooper, A. Dittmann, J. Kijima, H.-J. Kretzschmar, A. Kruse, R. Mareš, K. Oguchi, H. Sato, I. Stöcker, O. Šifner, Y. Takaishi, I. Tanishita, J. Trübenbach, and Th. Willkommen. The IAPWS Industrial Formulation 1997 for the Thermodynamic Properties of Water and Steam. *Transactions of the ASME*, 122:150–182, 2000.
[58] G. Wang, S. Zhang, M. Yu, H. Li, and Y. Kong. Investigation of the shock wave propagation characteristicsand cavitation effects of underwater explosion near boundaries. *Appl. Ocean Res.*, 46:40–53, 2014.
[59] A. B. Wood. *A textbook of sound*. G. Bell and Sons Ltd., London, 1930.
[60] W. F. Xie, T. G. Liu, and B. C. Khoo. Application of a one-fluid model for large scale homogeneous unsteady cavitation: The modified Schmidt model. *Computers and Fluids*, 35:1177–1192, 2006.
[61] W. F. Xie, T. G. Liu, and B. C. Khoo. The simulation of cavitating flows induced by underwater shock and free surface interaction. *Appl. Numer. Math.*, 57:734–745, 2007.
[62] G.-S. Yeom. Numerical study of underwater explosion near a free surface and a structural object on unstructured grid. *J. Mech. Sci. Technol.*, 29(10):4213–4222, 2015.
[63] A. Zein, M. Hantke, and G. Warnecke. Modeling phase transition for compressible two-phase flows applied to metastable liquids. *J. Comput. Phys.*, 229:2964–2998, 2010.
[64] A. Zein, M. Hantke, and G. Warnecke. On the modeling and simulation of a laser-induced cavitation bubble. *Int. J. Numer. Meth. Fluids*, 73(2):172–203, 2013.
[65] J. Zhu, T. Liu, J. Qiu, and B. C. Khoo. RKDG methods with WENO limiters for unsteady cavitating flow. *Computers and Fluids*, 57:52–65, 2012.